AD-A051 052

ARBRL-TR-02037

BRL

AD

TECHNICAL
LIBRARY

TECHNICAL REPORT ARBRL-TR-02037

NUMERICAL PREDICTIONS FOR IGNITION OF A CONFINED REACTIVE GAS

Douglas E. Kooker

January 1978

Approved for public release; distribution unlimited.

USA ARMAMENT RESEARCH AND DEVELOPMENT COMMAND
USA BALLISTIC RESEARCH LABORATORY
ABERDEEN PROVING GROUND, MARYLAND

DTIC QUALITY INSPECTED 3

Destroy this report when it is no longer needed.
Do not return it to the originator.

Secondary distribution of this report by originating or sponsoring activity is prohibited.

Additional copies of this report may be obtained from the National Technical Information Service, U.S. Department of Commerce, Springfield, Virginia 22161.

The findings in this report are not to be construed as an official Department of the Army position, unless so designated by other authorized documents.

The use of trade names or manufacturers' names in this report does not constitute indorsement of any commercial product.

REPORT DOCUMENTATION PAGE		READ INSTRUCTIONS BEFORE COMPLETING FORM
1. REPORT NUMBER TECHNICAL REPORT ARBRL-TR-02037	2. GOVT ACCESSION NO.	3. RECIPIENT'S CATALOG NUMBER
4. TITLE (and Subtitle) Numerical Predictions for Ignition of a Confined Reactive Gas		5. TYPE OF REPORT & PERIOD COVERED BRL Report 6. PERFORMING ORG. REPORT NUMBER
7. AUTHOR(s) Douglas E. Kooker		8. CONTRACT OR GRANT NUMBER(s)
9. PERFORMING ORGANIZATION NAME AND ADDRESS US Army Ballistic Research Laboratory (ATTN: DRDAR-BLP) Aberdeen Proving Ground, MD 21005		10. PROGRAM ELEMENT, PROJECT, TASK AREA & WORK UNIT NUMBERS 1T161102AH53
11. CONTROLLING OFFICE NAME AND ADDRESS US Army Armament Research & Development Command US Army Ballistic Research Laboratory (ATTN: DRDAR-BL) Aberdeen Proving Ground, MD 21005		12. REPORT DATE JANUARY 1978 13. NUMBER OF PAGES 68
14. MONITORING AGENCY NAME & ADDRESS(if different from Controlling Office)		15. SECURITY CLASS. (of this report) Unclassified 15a. DECLASSIFICATION/DOWNGRADING SCHEDULE

16. DISTRIBUTION STATEMENT (of this Report)

Approved for public release; distribution unlimited.

17. DISTRIBUTION STATEMENT (of the abstract entered in Block 20, if different from Report)

18. SUPPLEMENTARY NOTES

19. KEY WORDS (Continue on reverse side if necessary and identify by block number)

ignition of pre-mixed gases; Navier-Stokes equations for reacting flow; numerical integration

ssv/4589

20. ABSTRACT (Continue on reverse side if necessary and identify by block number) Ignition of a reactive gas in a closed chamber is investigated by numerically solving the one-dimensional, compressible Navier-Stokes Equations for a multi-species reacting flow. The full momentum equation is retained in order to model the influence of the finite-size chamber. Ignition is studied on a go/no-go basis when the external heat flux is interrupted. The results for a simple premixed reaction show a complex interaction with the acoustic modes, a hang-fire ignition separating go/no-go, and the possibility of a shock wave once ignition occurs. Dependence of ignition

time on external heat flux, activation energy, and other kinetic parameters is described.

TABLE OF CONTENTS

LIST OF TABLES

LIST OF FIGURES

LIST OF FIGURES (Continued)

NOMENCLATURE

a_r^*	reference speed of sound (cm/sec)
c_{p_i}	$c_{p_i}^* T_r^* / a_r^{*2}$; specific heat at constant pressure
D_{12}	$D_{12}^* / a_r^* L^*$; coefficient of diffusion (used in Fick's Law)
E	E^* / a_r^{*2}; total energy = $h + \frac{u^2}{2} - p/\rho$
$\hat{E}^*$	Activation energy (kcal/mole)
h	h^* / a_r^{*2}; enthalpy, $\sum_{i=1}^{N} Y_i h_i$
h_i	$\int_{T^o}^{T} c_{p_i} d\hat{T} + h_i^o$; enthalpy of species i (thermal + chemical)
h_i^o	heat of formation of species i at T^o
ΔH^*	heat of reaction (kcal/mole), $h_A^{o*} - 2h_B^{o*}$ for $A \rightarrow 2B$
k_g	$k_g^* T_r^* / \rho_r^* a_r^{*3} L^*$; thermal conductivity
L^*	reference length (cm)
M_i	molecular weight (gm/gm-mole)
N	total number of species
p	$p^* / \rho_r^* a_r^{*2}$; pressure
q_{wall}	$q^*_{wall} / \rho_r^* a_r^{*3}$; external heat flux, q^*_{wall} = cal/cm^2-sec
q_{wall_o}	constant portion of external heat flux
Re	$\rho_r^* a_r^* L^* / \mu_r^*$; reference value of Reynolds number
R_o	$R_o^* T_r^* / a_r^{*2}$; universal gas constant
t	$t^* a_r^* / L^*$; time
T	T^* / T_r^*; temperature
T_r^*	reference value of temperature (°K)

u	u^*/a_r^*; velocity
Y_i	ρ_i/ρ; mass fraction of species i
z	z^*/L^*; axial coordinate
Z^*	pre-exponential factor (sec^{-1})
μ	μ^*/μ_r^*; coefficient of viscosity
μ_R	$(4/3)\mu/Re$
μ_r^*	reference value of coefficient of viscosity (gm/cm-sec)
ρ	ρ^*/ρ_r^*; density
ρ_i	density of species i
ρ_r^*	reference value of density (gm/cm^3)
Θ	a constant, $0 \leqslant \Theta \leqslant 1$
$\tilde{\omega}_i$	$\tilde{\omega}_i^* L^*/\rho_{r_i}^* a_r^*$; chemical production rate of species i

Subscripts

i	pertaining to species i
j	location of grid point
r	reference value
t	derivative with respect to time
z	derivative with respect to axial coordinate

Superscripts

*	dimensional quantity
n	current time level
n+1	new time level

I. INTRODUCTION AND MOTIVATION

Any attempt to construct a mathematical model of solid propellant ignition and/or unsteady combustion is faced with the difficulty of describing the gas-phase reaction zone. Unless it can be assumed that solid-phase reactions dominate completely, a prediction of solid propellant decomposition rate is heavily dependent upon events occurring in the gas phase. Competition between convection, heat conduction, species diffusion, and chemical reaction rates will establish the instantaneous energy flux to the surface of the reactive solid. The ability to describe this interaction is a prerequisite for mathematical models designed for transient calculations.

The study of transient solid propellant combustion in Ref. 1 examined several combustion models which assume the flame region to be quasi-steady. This affords a tremendous simplification in the analysis, if it also can be assumed that the spatial distributions of heat release and chemical production rate are known and remain unchanged. The latter assumption effectively uncouples the energy equation from the species continuity equations, and thus any fixed distribution is hard to defend. Furthermore, the basic quasi-steady assumption is difficult to justify for problems related to a gun combustion chamber where the entire ignition and unsteady combustion process is completed within milliseconds.

Four recent models[2,3,4,5] of the solid propellant ignition process have analyzed the gas-phase reaction zone in much greater detail. These studies have led to considerable insight into the competing processes which control ignition of a reactive solid. However, all have dealt with a constant-pressure "isolated" ignition problem. The isolation is a consequence of applying vanishing gradient boundary conditions to the

---

[1] *Kooker, D. E., and Nelson, C. W., "Numerical Solution of Three Solid Propellant Combustion Models During a Gun Pressure Transient", BRL Report No. 1953 (AD #A035250), USA Ballistic Rsch Lab, APG, MD, Jan 77 (see also 12th JANNAF Combustion Meeting, Newport, RI, CPIA Publication 273, pp 173-197, Dec 75).*

[2] *Hermance, C. W., and Kumar, R. K., "Gas Phase Ignition Theory for Homogeneous Propellants Under Shock Tube Conditions", AIAA J., Vol. 8, No. 9, pp 1551-1558 (Sep 70).*

[3] *Kashiwagi, T., "A Radiative Ignition Model of a Solid Fuel", Comb. Sci. Tech., Vol. 8, pp 225-236 (1974).*

[4] *Bradley, H. H., Jr., "A Unified Theory of Solid Propellant Ignition, Part 1, Development of Mathematical Model", NWC TP5618 (Aug 74).*

[5] *Kindelan, M., and Williams, F. A., "Radiant Ignition of a Combustible Solid with Gas-Phase Exothermicity", Acta Astronautica, Vol. 2, No. 11/12 Nov/Dec 75).*

gas-phase dependent variables at an infinite distance from the propellant surface; thus, changes in the outside environment cannot influence the ignition process. Additionally, each analysis is constrained by various combinations of assumptions such as a unity Lewis number, negligible kinetic energy, multiple species with identical molecular weights and specific heats, etc.

The current study is motivated by a desire to model the ignition and unsteady combustion process of an end-burning solid propellant grain confined in a one-dimensional chamber, as shown in Fig. 1a. The model must be sufficiently general to allow variable transport properties, various chemical decomposition schemes, etc., without the restriction of constant pressure. The objective is two-fold: (a) predict the instantaneous regression rate of the reactive solid as a function of the self-generated pressure, and (b) look for potential instabilities in both regimes--ignition and unsteady combustion.

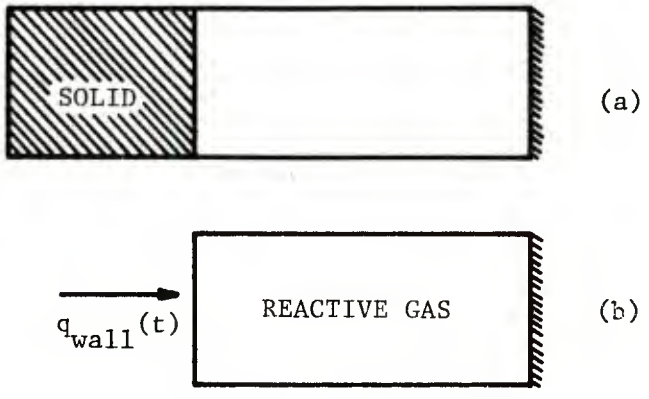

Figure 1. Problem Configurations - (a) Solid Propellant in Closed Chamber; (b) Reactive Gas in Closed Chamber

The present investigation is the first step in the above model and has the limited objective of describing the ignition sequence of a reactive gas confined in a rigid, one-dimensional chamber. As shown in Fig. 1b, one boundary is assumed to be insulated and the other is subjected to an externally-prescribed, time-dependent heat flux. The imposed heat flux, as used here, serves as the ignition stimulus and is not intended to represent the response of the solid in the full propellant ignition problem of Fig. 1a. The remainder of this report is concerned with the solution of the gas-phase ignition problem shown in Fig. 1b.

II. ANALYSIS

The gas-phase ignition problem described above requires the numerical solution to the one-dimensional, time-dependent, compressible

Navier-Stokes Equations for a multi-species reacting flow field. To correctly model the influence of the finite-size chamber, the system must retain the full momentum equation, as opposed to the trivial constant-pressure form. At no time will the analysis employ an externally specified value of "$T_{ignition}$"; thus, no artificial boundary is drawn between ignition and unsteady combustion. Ignition will be determined by a go/no-go response when the external heat flux is terminated.

Assumptions

The reactive gas confined in the chamber is assumed to be a mixture of perfect gases, each of which may have a different molecular weight, specific heat capacity, and heat of formation. It is assumed that the mixture viscosity, thermal conductivity, and species diffusion coefficients can be described at the molecular level, i.e., all transport is laminar. Admittedly, turbulent transport is the dominant mode in many combustion situations. However, the gas-phase ignition problem posed here should not be controlled by turbulence. In the event of a violent unsteady flame propagation in the chamber, this assumption would have to be re-examined. The numerical solution procedure assumes variable laminar transport properties, with no constraints on the magnitude or variability of the mixture Lewis number or Prandtl number. The influence of radiation, gravity, bulk viscosity, the Dufour effect, the Soret effect, and diffusion due to pressure gradients will be neglected.

The current results are based on the additional assumption that the chamber initially contains a reactive gas composed of the single species A, capable of undergoing the one-step, irreversible reaction

$$A \rightarrow 2B.$$

Fick's Law is then used to describe the diffusion mass flux in this binary system. It should be noted that extending Fick's Law to a generalized multi-component mixture, and then assigning unequal diffusion coefficients, will lead to a violation of the basic identity that the sum of the diffusion mass fluxes must be zero. Although this has been done[6,7], the

---

[6] *Rivard, W. C., Farmer, O. A., and Butler, T. D., "RICE: A Computer Program for Multicomponent Chemically Reactive Flows at All Speeds", LA-5812, Los Alamos Scientific Laboratory, Los Alamos, NM, Mar 75.*

[7] *Kothari, A. P., Anderson, J. D., Jr., and Jones, E., "Navier-Stokes Solutions for Chemical Laser Flows", AIAA J., Vol. 15, No. 1, pp 92-100 (Jan 77).*

correct procedure requires the solution of the coupled equations relating all diffusion mass fluxes and mass fraction gradients, as described by Edelman[8].

Governing Equations

Based on the foregoing assumptions, the conservation equations in an inertial frame of reference can be written as:

Global Continuity
$$\rho_t + (\rho u)_z = 0 \tag{1}$$

Momentum
$$\omega_t + [\omega u + p]_z = [\mu_R (\frac{\omega}{\rho})_z]_z \tag{2}$$

Energy
$$(\rho E)_t + [\omega E + pu]_z = \left\{ k_g T_z + \mu_R u u_z + (\sum_{i=1}^{N} h_i \rho D_{12} Y_{i_z}) \right\}_z \tag{3}$$

Species Continuity
$$\rho Y_{i_t} + \omega Y_{i_z} = (\rho D_{12} Y_{i_z})_z + \tilde{\omega}^i \qquad i=1,\ldots,N-1 \tag{4}$$

State
$$p = \rho R T \quad , \quad R \equiv R_o \sum_{i=1}^{N} (Y_i / M_i)$$

$$h = \sum_{i=1}^{N} Y_i h_i \quad , \quad h_i = \int_{T^o}^{T} c_{p_i} d\hat{T} + h_i^o \tag{5}$$

where $\omega \equiv \rho u$, $E \equiv h + \frac{u^2}{2} - p/\rho$, $Y_i = \rho_i / \rho$

Equations (1) - (3) are solved numerically in their strict conservation form. Attempts to solve the species continuity equation written in terms of partial densities led to numerical instabilities when forming a mass fraction with a value very close to unity. The origin of this instability appears to be machine inaccuracy in division of two nearly identical numbers, and is not attributable to the stiffness of the equation. Use of the form shown in Eq. (4) eliminated the difficulty.

The common practice of transforming the axial coordinate (using an integral of density) to eliminate direct dependence on the global continuity equation is unworkable here because the computational domain is enclosed by two boundaries at finite locations.

---

[8] *Edelman, R. B., Fortune, O. F., and Weilerstein, G., "An Analytical and Experimental Investigation of Gravity Effects Upon Laminar Gas Jet-Diffusion Flames", 14th Symposium (International) on Combustion, Aug 72, Penn State University, pp 399-412.*

Boundary Conditions

Boundary values of the dependent variables must be specified at both the heated boundary, z=0, and the insulated boundary, z=1 (see Fig. 2).

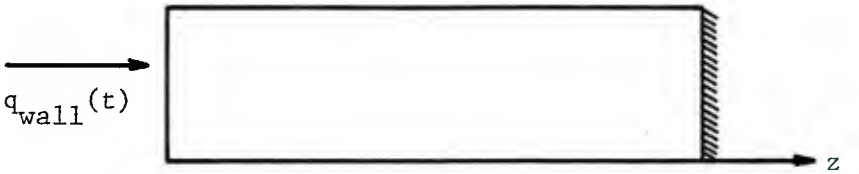

	$z = 0$	$z = 1$	
(a)	$u \equiv 0$	$u \equiv 0$	
(b)	$Y_{i_z} = 0 \quad i=1,\ldots N-1$	$Y_{i_z} = 0$	(6)
(c)	$T_z = -q_{wall}/k_g$	$T_z = 0$	

Figure 2. Physical Boundary Conditions

The assumption of impenetrable walls requires the mean flow velocity to vanish at z=0 and z=1 [Eq. (6a)]. The individual species velocities must also vanish at the solid boundary, which means that all diffusion velocities are zero. Since by Fick's Law the diffusion velocity is linearly dependent upon the spatial gradient of the mass fraction, each mass fraction gradient must vanish at z=0 and z=1 [Eq. (6b)]. Combining Eqs. (6a) and (6b) with the energy balance at the boundaries results in a zero temperature gradient at z=1 and a time-dependent temperature gradient at z=0 governed by $q_{wall}(t)$ [Eq. (6c)]. At each boundary, there are N+3 dependent variables, but only N+2 conditions given by Eq. (6) along with the equation of state. However, no physical boundary condition is missing. The situation is directly analogous to the simpler, inviscid acoustic problem at a boundary; a value of the velocity perturbation (or an equivalent admittance condition) can be specified but the value of the pressure perturbation must follow from the solution. To specify both values would over-determine the system of equations.

The numerical solution procedure requires values of all dependent variables at both boundaries for every time step. In a complex system of equations, the manner in which the "extraneous" boundary values are determined is usually the difference between success and failure. An accurate method to solve the inviscid acoustic problem is based on the fact that the system of equations is hyperbolic. Because of the finite propagation velocity, one characteristic line in the t-z plane will intersect the boundary at the new time level. The compatibility condition along this line provides the missing information which relates the unknown boundary values to the known solution at the previous time level.

In the present gas-phase ignition problem, the governing equations are parabolic. All characteristic directions have essentially collapsed to the single line t=constant, which implies an infinite speed of propagation. The potential benefit from a method-of-characteristics solution at the boundary is now lost.

The present investigation attempted several different methods to determine the boundary value of pressure consistent with the interior numerical solution. The only successful one is based on the idea of mechanical equilibrium at the boundary. Since the mean velocity is constrained to be zero at all times, the momentum equation reduces to the statement that the gradient of the stress tensor must vanish. Thus, at the boundary, the gradient of thermodynamic pressure must balance the gradient of the viscous normal stress, viz.,

$$p_z = (\mu_R u_z)_z \tag{7}$$

Equation 7 is enforced at a boundary by fitting a cubic profile (in velocity and pressure) through the adjacent nearest neighbors, and appropriately differentiating. This provides the value of pressure, and then the value of density follows directly from the equation of state [Eq. (5)].

The boundary conditions are completed by specifying the time-dependent heat flux imposed at z=0. All computations discussed in the present study are based on $q_{wall}(t)$ shown in Fig. 3, where the duration of heating is altered by varying the cut-off time, t_{mq}. The shut-down portion of the heating profile (after t_{mq}) is necessary to keep a discontinuous gradient from destroying the numerical solution; its shape remained unchanged throughout the study. Unless otherwise stated, the constant portion of the heating curve was held at the value 10 cal/cm^2-sec. Note that for $t > t_{mq} + 5$, the heated wall becomes adiabatic.

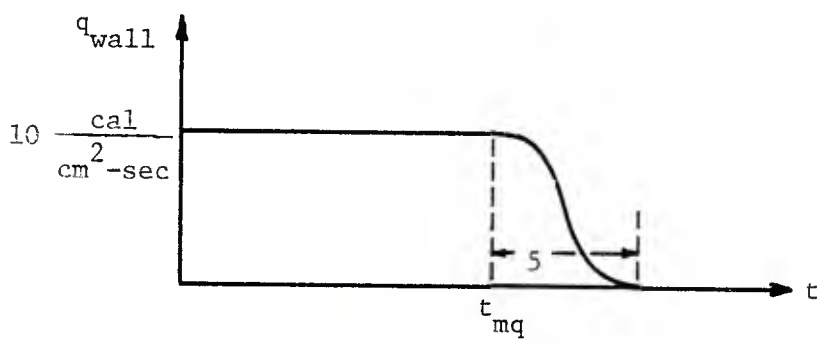

Figure 3. Time-Dependent Heat Flux Imposed at z=0

Method of Solution

The numerical integration technique used to solve Eqs. (1) - (4) is constructed on the basis of a control volume of length Δz centered about each grid point (see Fig. 4).

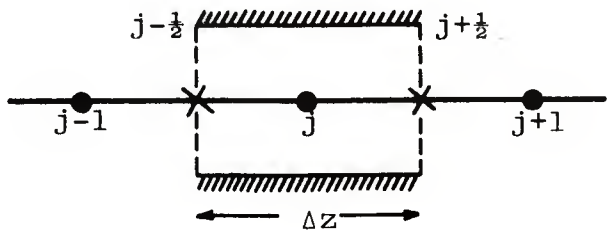

Figure 4. Control Volume Nomenclature

Each term in the equation, other than the time derivative, is weighted between its value at the old time level "n" and the new time level "n+1". Using global continuity [Eq. (1)] as an example,

$$\frac{\rho_j^{n+1} - \rho_j^n}{\Delta t} + \frac{\theta}{\Delta z}\left(\rho u_{j+\frac{1}{2}} - \rho u_{j-\frac{1}{2}}\right)^{n+1} + \frac{1-\theta}{\Delta z}\left(\rho u_{j+\frac{1}{2}} - \rho u_{j-\frac{1}{2}}\right)^{n} = 0 \qquad (8)$$

where θ is a constant, $0 \leqslant \theta \leqslant 1$, and the subscripts indicate grid point location. The accuracy of the integration is $O(\Delta t^2)$ if $\theta=\frac{1}{2}$. However, with the competing effects of convection and diffusion, stability can be assured only when $\theta > \frac{1}{2}$. All solutions discussed in this report are based on $\theta=0.55$. Values of the dependent variables are stored only at the integer grid point location; values required at the midpoints are found from

$$\rho u_{j+\frac{1}{2}} = \tfrac{1}{2}(\rho u_{j+1} + \rho u_j), \text{ etc.} \qquad (9)$$

Similarly, flux terms which depend on a spatial gradient are represented as

$$k_g T_z \Big|_{j+\frac{1}{2}} = \tfrac{1}{2}(k_{g_{j+1}} + k_{g_j})\left(\frac{T_{j+1} - T_j}{\Delta z}\right) \qquad (10)$$

using the internal heat flux as an example. This procedure insures strict conservation, i.e., the flux value entering control volume j+1 across the interface located at $j+\frac{1}{2}$ will be exactly the value which left control volume j across the same interface.

Equations (2) - (4) are each written in a form analogous to Eq. (8), such that the terms representing time storage, convection, diffusion, and production are coupled at the new time level "n+1". The result, after applying the boundary conditions, is a tri-diagonal matrix which can be inverted with the standard Thomas Algorithm. The solution then proceeds by successive substitution, not quasi-linearization. A series of tri-diagonal matrix inversions is performed in the following sequence, where each step incorporates the latest dependent variable estimates from the previous steps:

1. Solve the species continuity equations for the Y_i's,

2. Solve the energy equation for the E's,

3. As a provisional step, solve the global continuity equation for the ρ's and update the pressure array,

4. Solve the momentum equation for the ω's,

5. Re-solve the global continuity equation for the ρ's and again update the pressure array.

Steps 1-5 constitute one iteration; the values of the dependent variables at the new time level are taken to be those obtained on the third iteration. Of the flow field points investigated, the third iteration produced convergence to at least five significant digits.

Stability of this integration could be maintained only by observing the well-known Courant condition,

$$\Delta t < \Delta x/(a+u)_{max}$$

which is normally applicable to explicit techniques. Furthermore, the cell Reynolds number limitation,

$$Re_{cell} \equiv uRe\Delta z < 2$$

became a major barrier. All attempts to circumvent these two restrictions ended in failure. The difficulty stems primarily from the type of problem posed here. A system of coupled parabolic partial differential equations, exhibiting an infinite speed of propagation (all characteristic directions collapse to t=constant), is solved between two fixed boundaries. The closed computational domain traps (and retains) numerical errors as well as the desired physical quantitites. Furthermore, rapid heating of the chamber excites nonlinear acoustic oscillations in the gas which change significantly on a short time scale. This combination presents a formidable challenge to any numerical method based on large time steps.

III. RESULTS

Numerical predictions for ignition behavior are presented for a simple two-species system representing the ultimate in a premixed reaction. Initially, the chamber contains only species A which is capable of the single, one-step, irreversible reaction,

$$A \rightarrow 2B.$$

As would be the case for an elementary reaction, the reaction rate is assumed linearly proportional to the concentration of A. Hence, the chemical production rate term required in Eq. (4) can be written as

$$\tilde{\omega}^A = -Z^* \rho Y_A (L^*/a_r^*) \exp[-\hat{E}^*/R_o^* T^*].$$

In keeping with the simplicity of this example, the thermal conductivity, viscosity, diffusion coefficient, and specific heats were all held constant at the representative values shown in Table 1.

Table 1. Parameters Held Constant

$M_A^* = 30$ gm/gm-mole	$M_B^* = 15$ gm/gm-mole
$c_{p_A}^* = .331$ cal/gm-°K	$c_{p_B}^* = .662$ cal/gm-°K
$k_g^* = 2.0 \times 10^{-4}$ cal/cm-sec-°K	
$D_{12}^* = 5.0 \times 10^{-1}$ cm^2/sec	
$\mu_r^* = 5.0 \times 10^{-4}$ gm/cm-sec ; $\mu = 1$	
$L^* = 2.5 \times 10^{-2}$ cm	
$a_r^* = 3.2238 \times 10^4$ cm/sec	
$T_r^* = 300$ °K	
Re = 1965.4	

A parametric study was conducted to estimate the influence of the three important kinetic parameters, Z^* the pre-exponential factor, $\hat{E}^*$ the activation energy, and ΔH^* the heat of reaction. The values considered are listed in Table 2.

Table 2. Results of Parametric Study
(q^*_{wall} = 10 cal/cm^2-sec)

Case	$\hat{E}^*$ kcal/mole	Z^* sec^{-1}	ΔH^* (exothermic) kcal/mole	t_{mq} at go/no-go (n-d)
Std.	35	10^{13}	35	127.87
CV1	35	10^{12}	35	174.7
CV2	35	10^{12}	25	185.4
CV3	35	10^{12}	30	179.3
CV4	35	10^{13}	30	131.0
CV5	35	10^{14}	30	97.6
CV6	30	10^{12}	30	115.8
CV7	30	10^{13}	30	83.0

The results to follow are displayed in machine-drawn plots, constructed by connecting two points with a straight line segment. None of the curves were smoothed or fitted with polynomials or splines. The non-dimensional axial distance, $0 \leq z \leq 1$, is divided into 50 cells.

For reference purposes, Fig. 5 shows the temperature distribution in the chamber for the special case when q_{wall} is held constant at 10 cal/cm^2-sec and the reaction rate is set to zero. The parameter values listed on the right-hand side of the figure are non-dimensional times from the onset of heating; one non-dimensional time unit is the time required for a small amplitude disturbance to travel the length of the chamber, assuming a uniform temperature of 300°K and $Y_A \equiv 1$. Initial conditions are $u^* \equiv 0$, $p^* = 1$ atm., and $Y_A \equiv 1$. The results show that 850°K is the maximum temperature achieved during a heating time of 145 time units when species A is inert.

Figure 6 shows the temperature distribution in the chamber for the kinetic parameters denoted as the standard case. The heating rate remained constant at 10 cal/cm^2-sec. The temperature at z=0 exceeds 850°K at a time of 128, and the distribution shows evidence of the classic

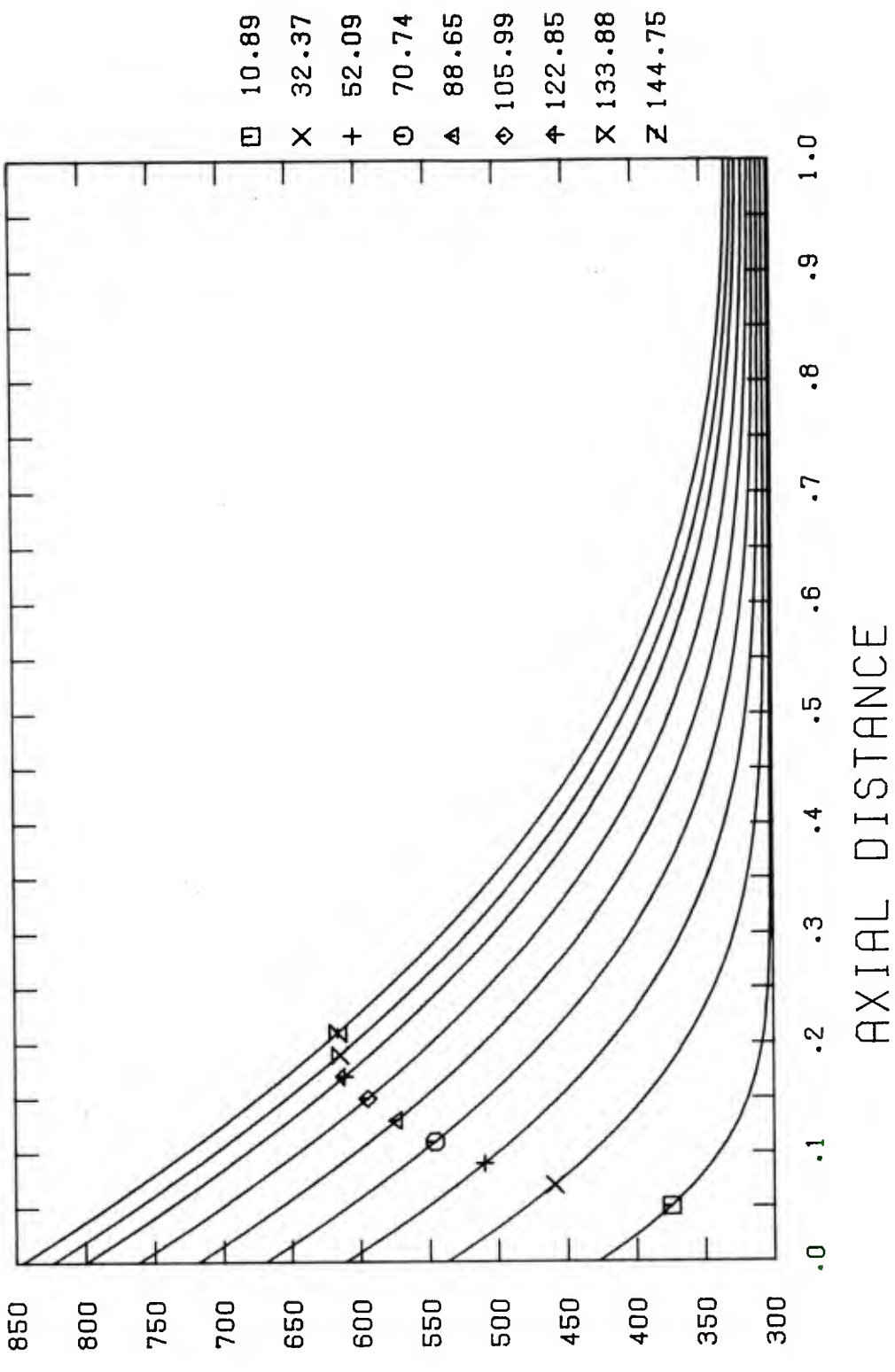

Figure 5. Temperature Distribution for Standard Case (No Reaction)

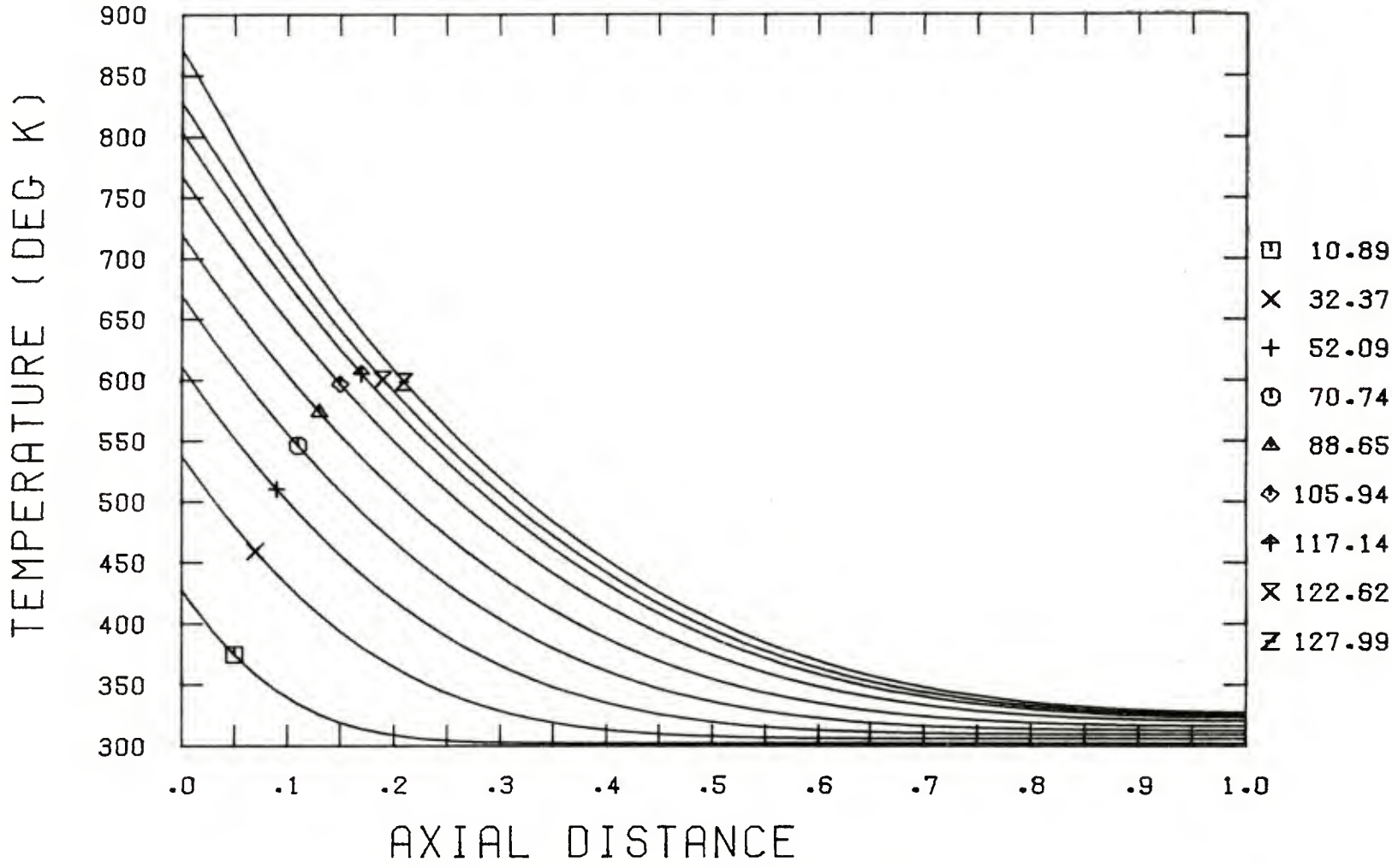

Figure 6. Temperature Distribution for Standard Case

"bulge" near the heated wall as discussed by Merzhanov and Averson[9]. This indicates the onset of the reaction. These temperature profiles, however, give no indication of the oscillatory nature of the confined gas. Rapid heating of the chamber leads to a thermally-driven convection process which creates the velocity oscillation pattern shown in Fig. 7. The plot shows the development of the wave over one-half of the cycle; as indicated by the shape of the profile, the frequency is close to that of the fundamental. Note that all velocities are positive. Hence, hot gas is continuously carried away from the heated end of the chamber. This is verified by the development of the density distribution shown in Fig. 8. The counterpart of the bulge in the temperature distribution near z=0 is visible in the density distribution at t≈128. The extent of the chemical reaction at this time can be visualized with the reactant mass fraction distribution displayed in Fig. 9. The results indicate the reaction at the boundary is approximately two percent complete.

As a first step toward establishing the critical go/no-go ignition point, the time t_{mq} which begins the shut-down portion of the external heat flux curve (see Fig. 3) was set to 127.0. The temperature distribution in Fig. 10 clearly shows the reaction was not self-sustaining, and the temperature profiles decay between two adiabatic walls. An interesting aspect of this cooling process is the effect on the velocity oscillation pattern. The pressure near the heated boundary immediately senses the falling temperatures and sends an expansion wave across the chamber. This expansion wave inverts the velocity oscillation to create the pattern in Fig. 11, which shows the development of the distribution during one-half of the oscillation cycle. The negative velocities mean the direction of the flow is toward the heated boundary; thus, cold gas is brought in to help "put out the fire." This is again confirmed by the density distribution displayed in Fig. 12. The progress of the reaction can be followed in Fig. 13 which shows the reactant mass fraction distribution during the same time interval. The reaction near the wall continues to three percent completion (at t≈133) even though the temperatures are decreasing, but then convection and diffusion begin to dominate. The result is an increase in the mass fraction of A near the wall, as the product B is spread throughout the chamber.

The behavior near the critical ignition point can be seen more clearly by plotting the temperature of the gas at z=0 as a function of time, for a series of runs varying only t_{mq}. Such a plot is shown in Fig. 14. The extreme sensitivity of this pre-mixed reaction to the cut-off time of the external stimulus is evident; the critical time of 127.87 leads to a hang-fire situation where the runaway reaction occurs 36 time units after t_{mq}. A nearly identical phenomenon was predicted

---

[9] *Merzhanov, A. G., and Averson, A. E., "The Present State of the Thermal Ignition Theory: An Invited Review", Comb. Flame, Vol. 16, pp 89-124 (1971).*

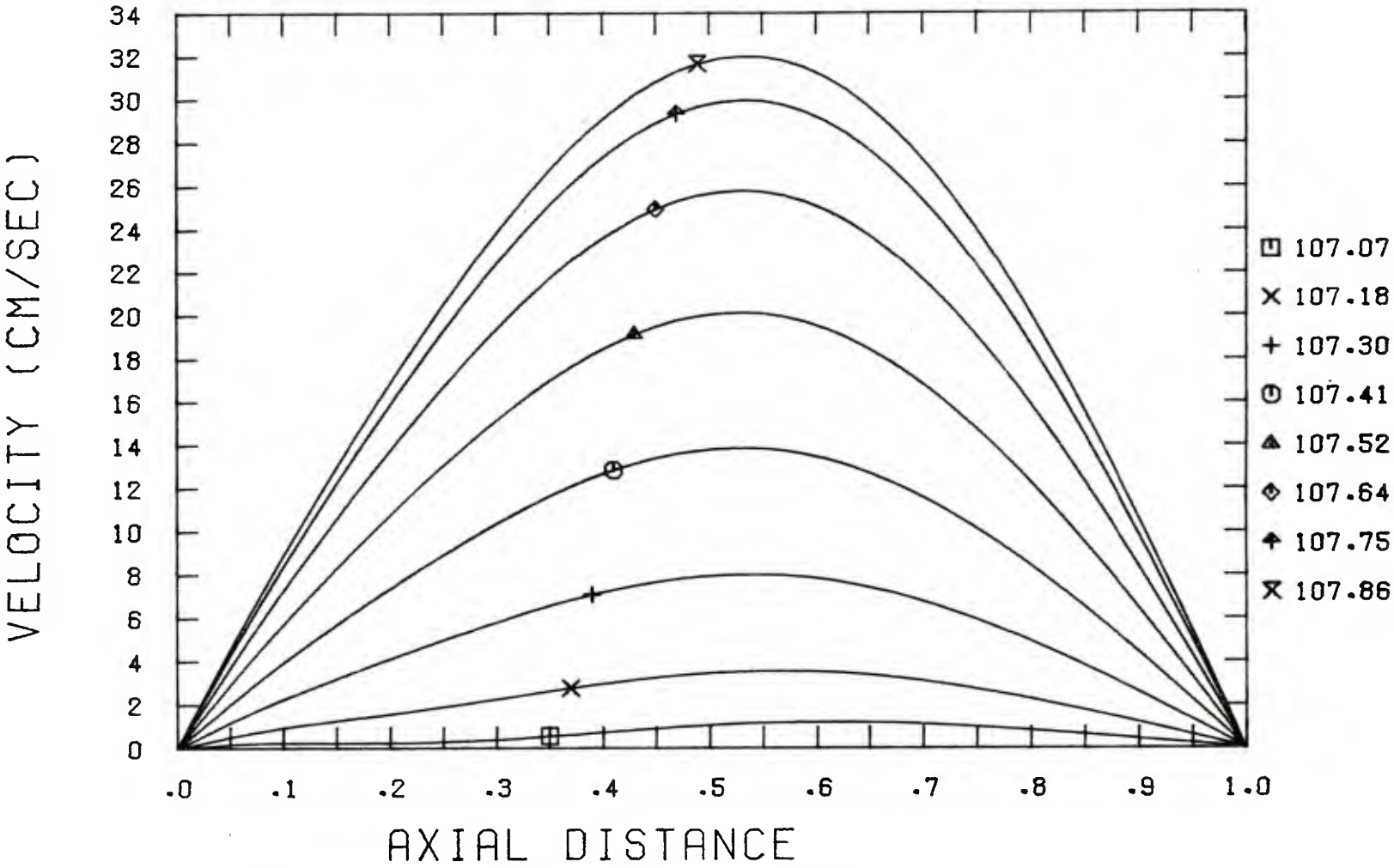

Figure 7. Velocity Distribution for Standard Case At Time ~107

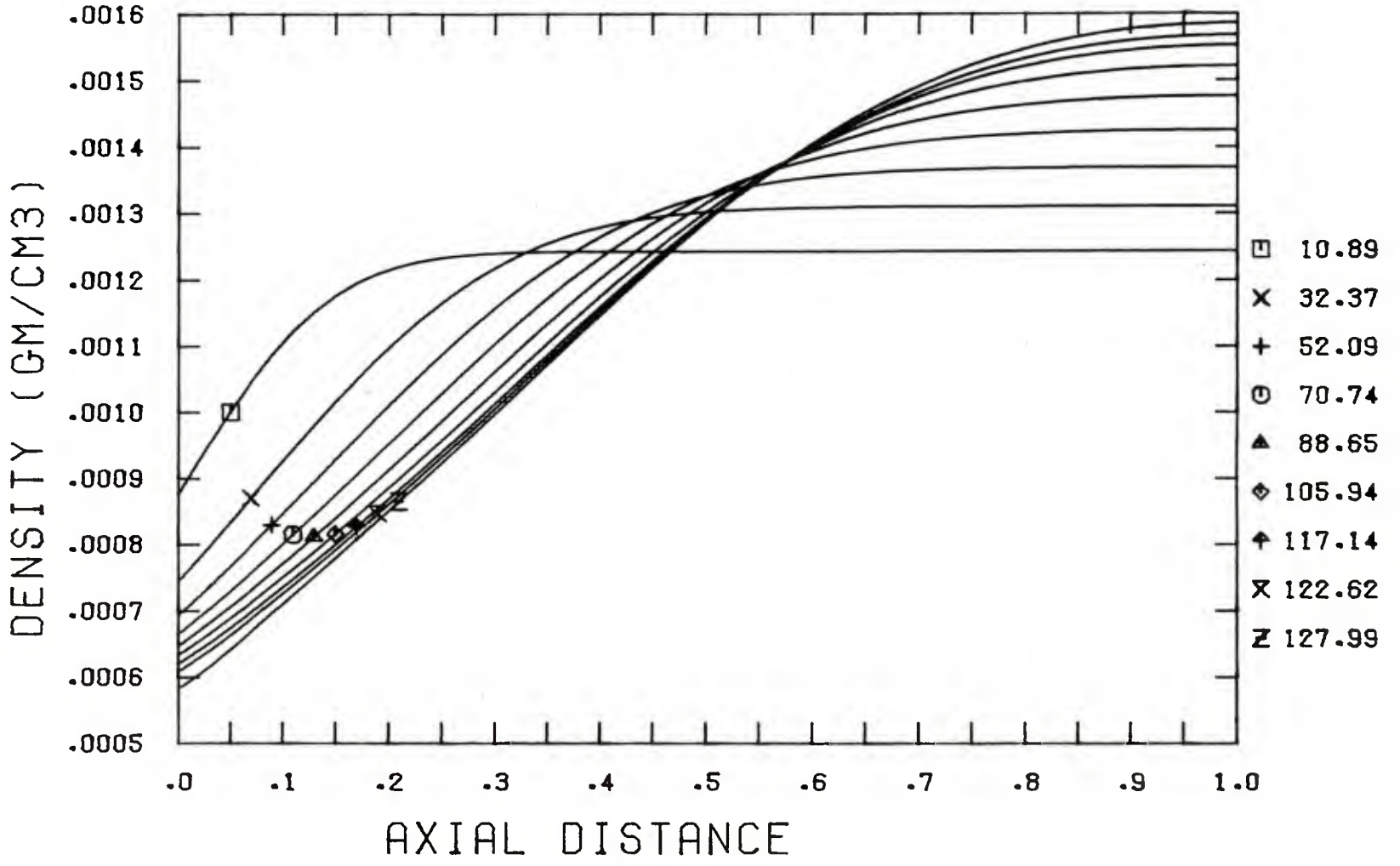

Figure 8. Density Distribution for Standard Case

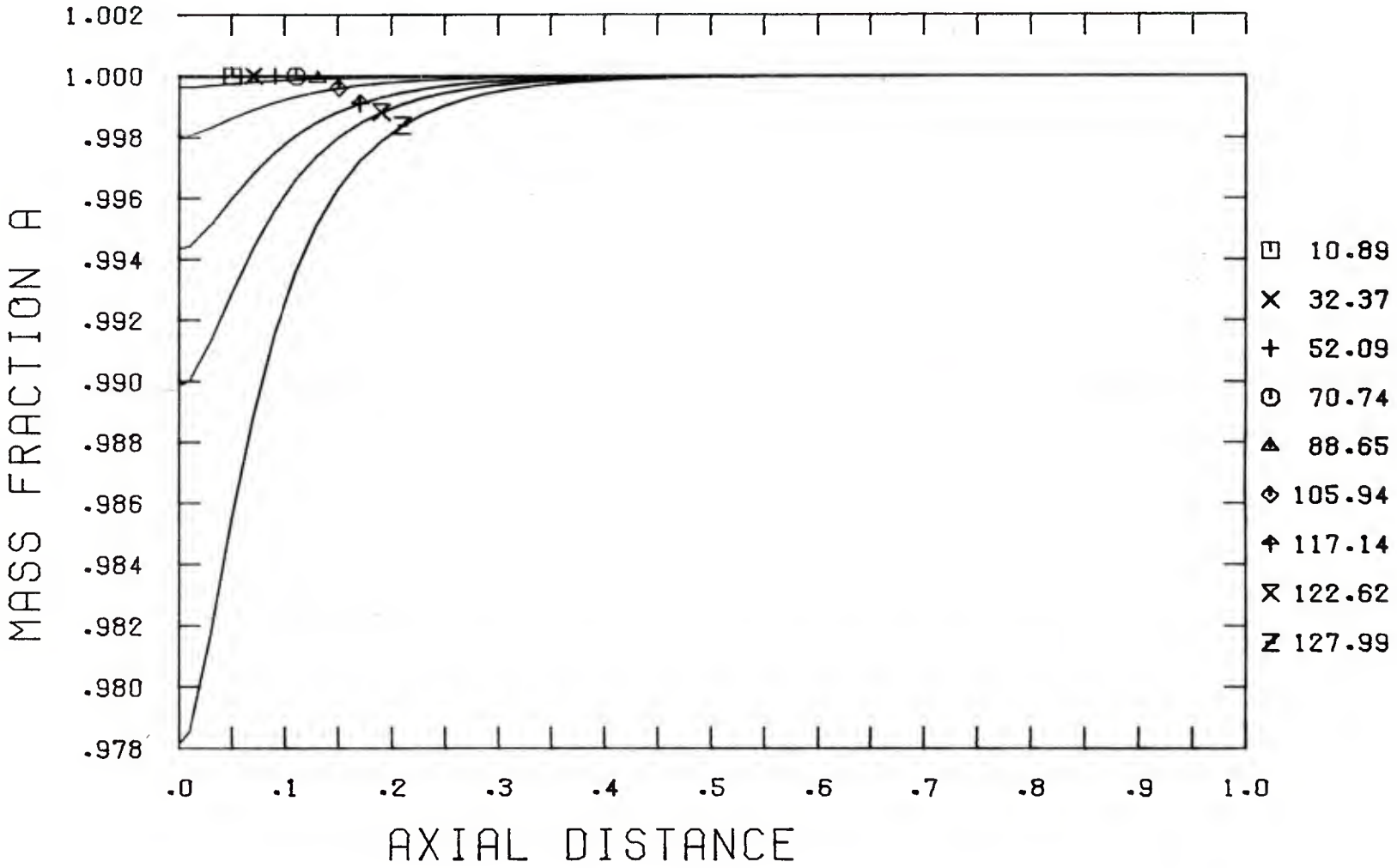

Figure 9. Reactant Mass Fraction Distribution for Standard Case

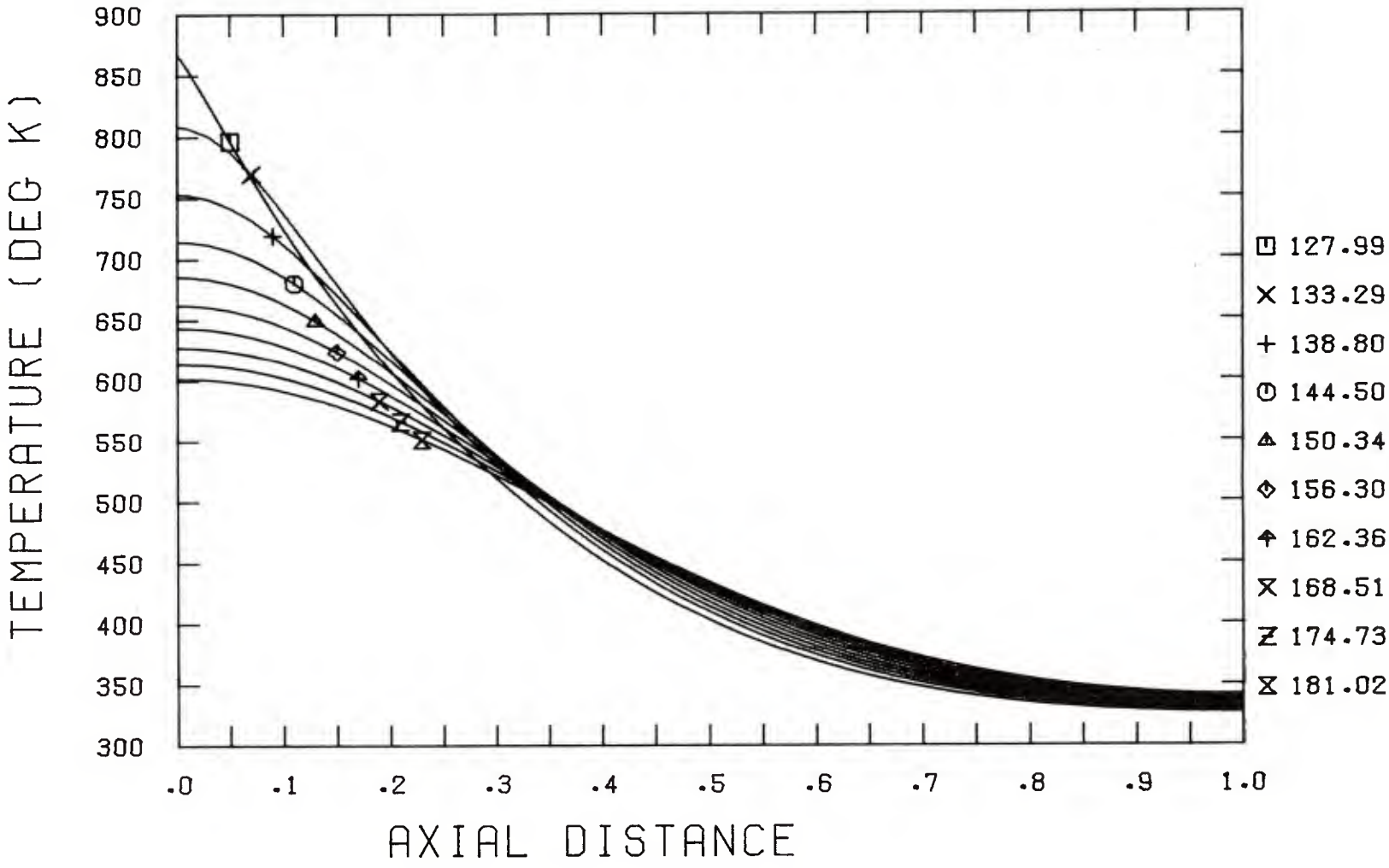

Figure 10. Temperature Distribution for Standard Case (t_{mq}=127.0)

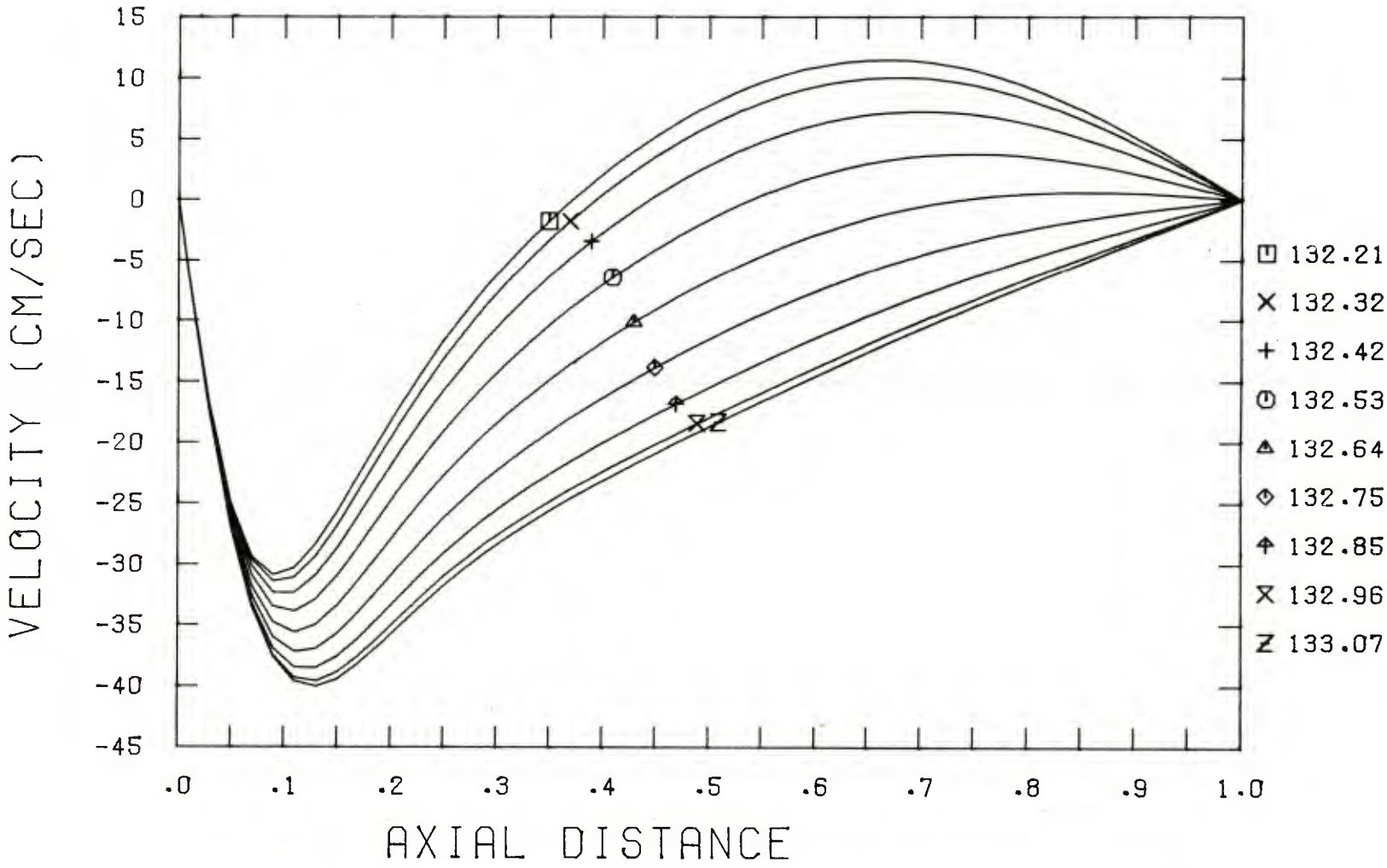

Figure 11. Velocity Oscillation Pattern for Standard Case (t_{mq}=127.0) At Time ~132

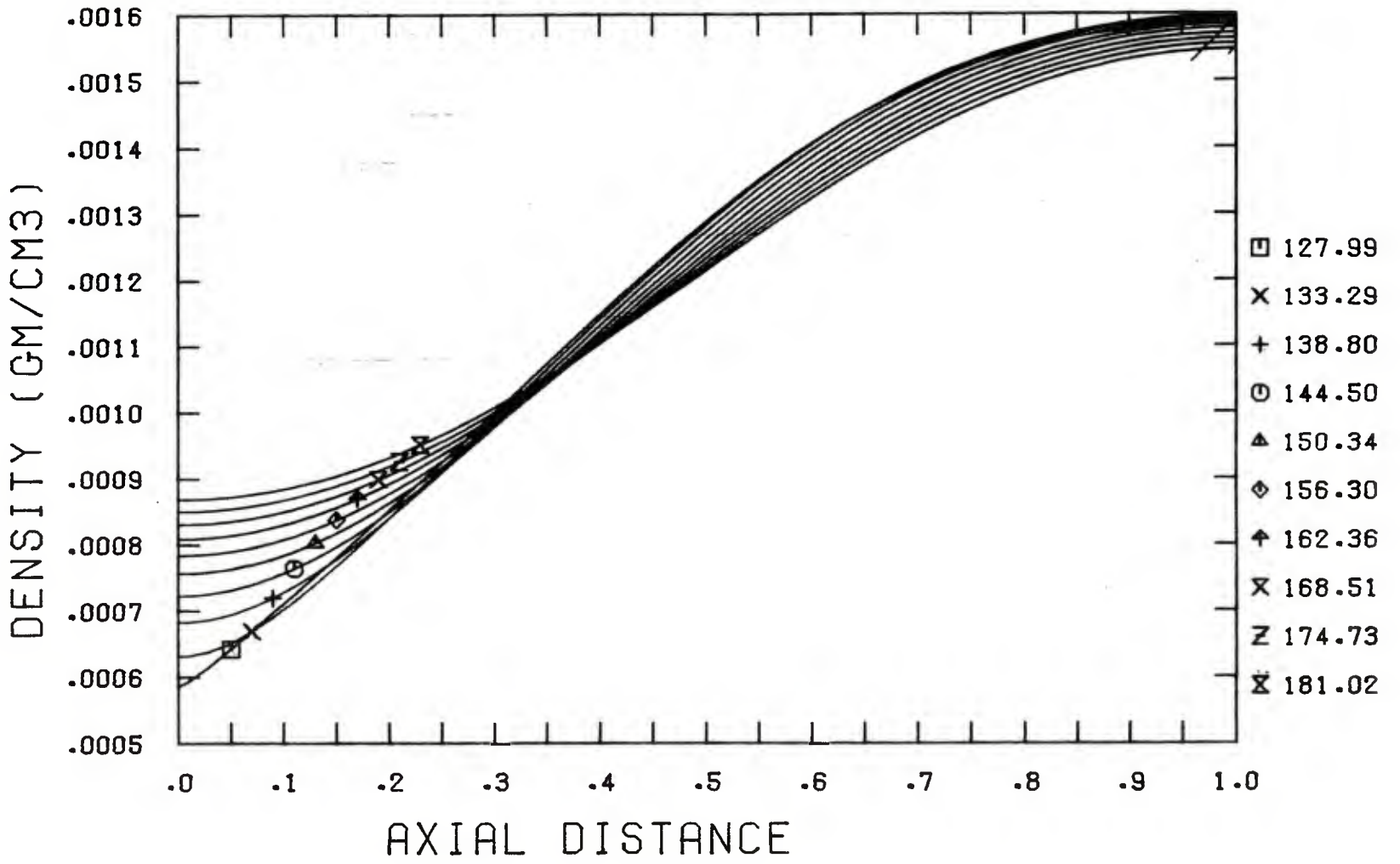

Figure 12. Density Distribution for Standard Case (t_{mq}=127.0)

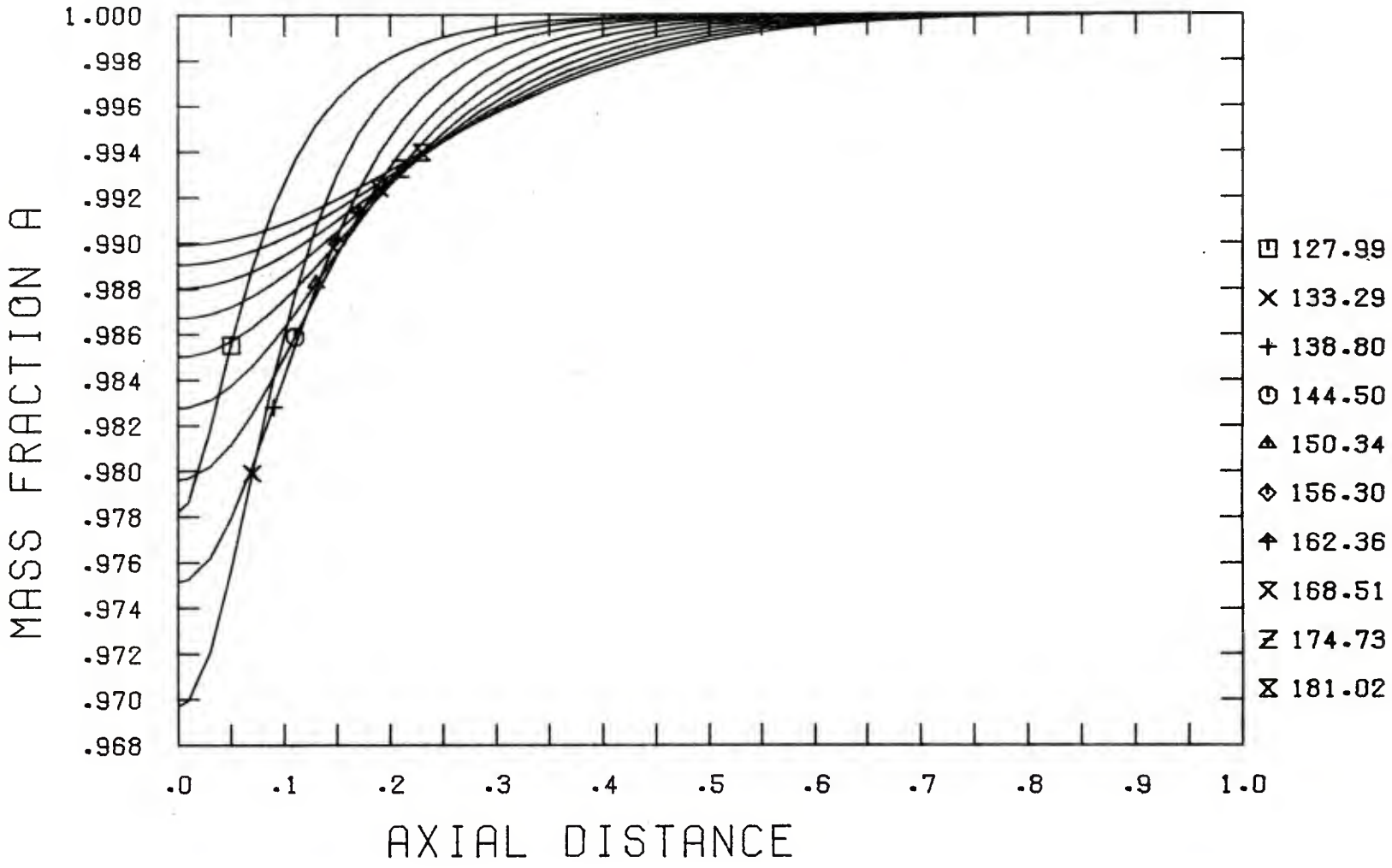

Figure 13. Reactant Mass Fraction Distribution for Standard Case (t_{mq}=127.0)

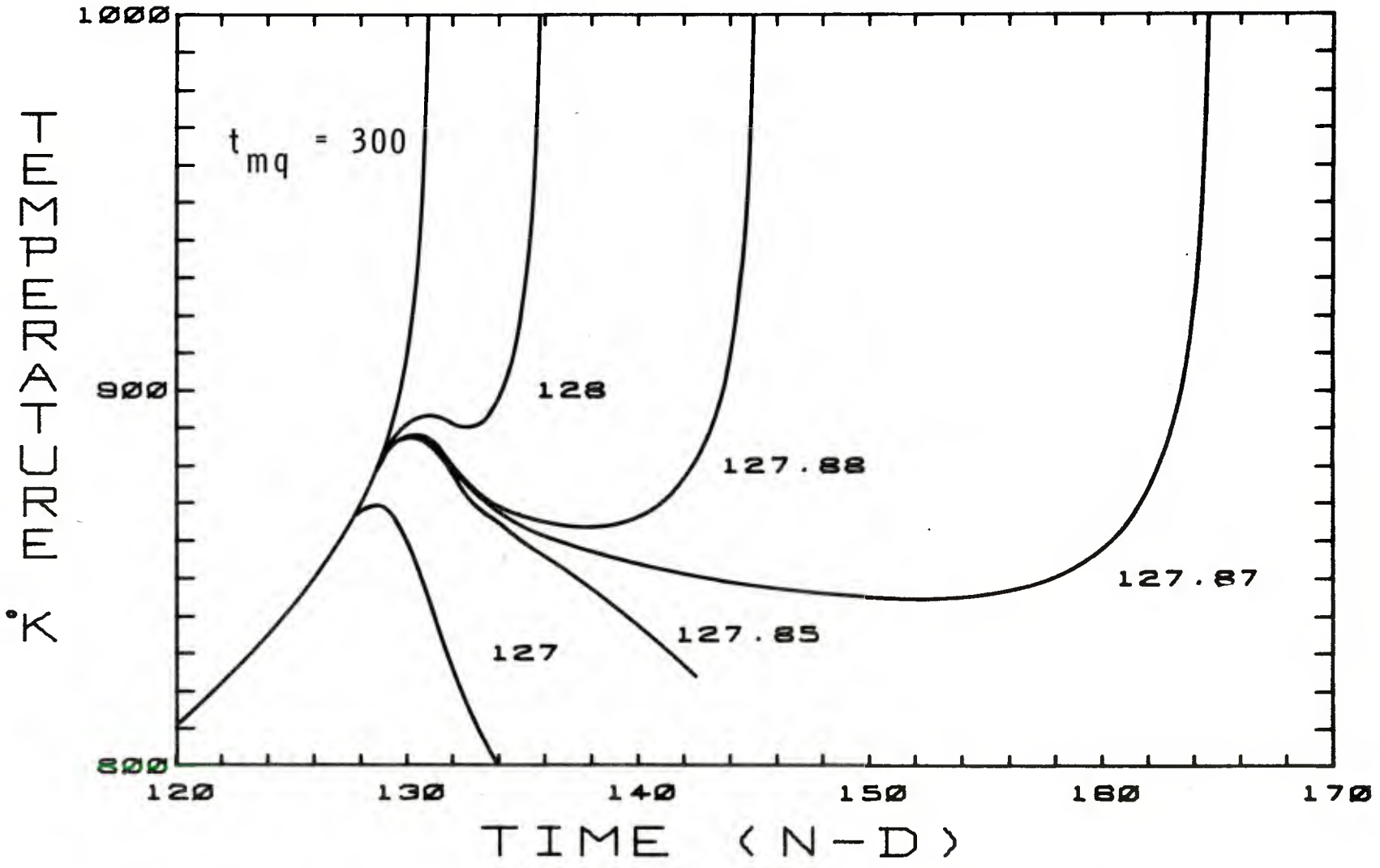

Figure 14. Temperature-Time History At Heated Wall (Varying t_{mq}) for Standard Case

by Bradley[10] in his ignition study of a reactive solid with no contribution from the gas-phase.

Evidence that the runaway reaction is self-sustaining after the long hang-fire (t_{mq}=127.87) is given by the temperature distribution plotted in Fig. 15 at a time of approximately 164. The results indicate a rapid rise to nearly 2600°K as the flame forms at the z=0 boundary. In this short time interval, the temperature is increasing much faster than the density can decrease. Hence, a significant change in pressure should occur. This is indeed the case, as shown in Fig. 16. The rapidly increasing pressure profiles coalesce into a shock wave. Unfortunately, the numerical integration method is sensitive to the fact that continuous differential equations cannot be integrated directly across a discontinuity and this halts the solution. It is concluded, however, that successful ignition of a pre-mixed gas with the kinetic parameters of the standard case will lead to a detonation wave.

The rapid heat release which drives the shock wave formation, displayed in Figs. 15 and 16, has a dramatic influence on the gas velocity oscillation pattern in the chamber. This is shown in the multiple plots of Fig. 17 for the standard case when t_{mq}=128.0 (see Fig. 14 for the wall temperature-time history). Temperature and velocity distributions are plotted in Figs. 17(a) and 17(b) for the time interval when the runaway reaction is just beginning. At the time of 133.14, the velocity distribution is a low amplitude oscillation pattern similar to that shown in Fig. 7. However, the internal heat generation near the z=0 boundary creates an increasing temperature and pressure field which halts the oscillation and forces a monotonically swelling velocity profile. This continues at an accelerated pace, as shown in Figs. 17(c) and 17(d), and the maximum velocity moves closer toward the boundary. This will become a "blast-wave" velocity profile which must follow behind the forming detonation wave.

A set of kinetic parameters which does not create a detonation wave can be found in Case CV2. Compared to the standard case, the pre-exponential factor is reduced by a factor of 10 and the exothermic heat release is 10 kcal/mole lower. This combination significantly increases the time to ignition as shown in the temperature-time history plot of Fig. 18. Once ignited, this case produces a much less severe temperature distribution as shown in Fig. 19. The flame temperature is approximately 1800°K, compared to 2600°K for the standard case. Figure 20 shows the reactant mass fraction distribution as the flame is forming. An estimate of the thickness of this pre-mixed flame is about 50 microns. This may be reasonable considering that a complex methane-air diffusion flame is 600-800 microns. Figure 21 is a plot of the pressure distribution during flame formation. The last profile is similar to the

---

[10] *Bradley, H. H., Jr., "Theory of Ignition of a Reactive Solid by Constant Energy Flux", Comb. Sci. Tech., Vol. 2, pp 11-20, (1970).*

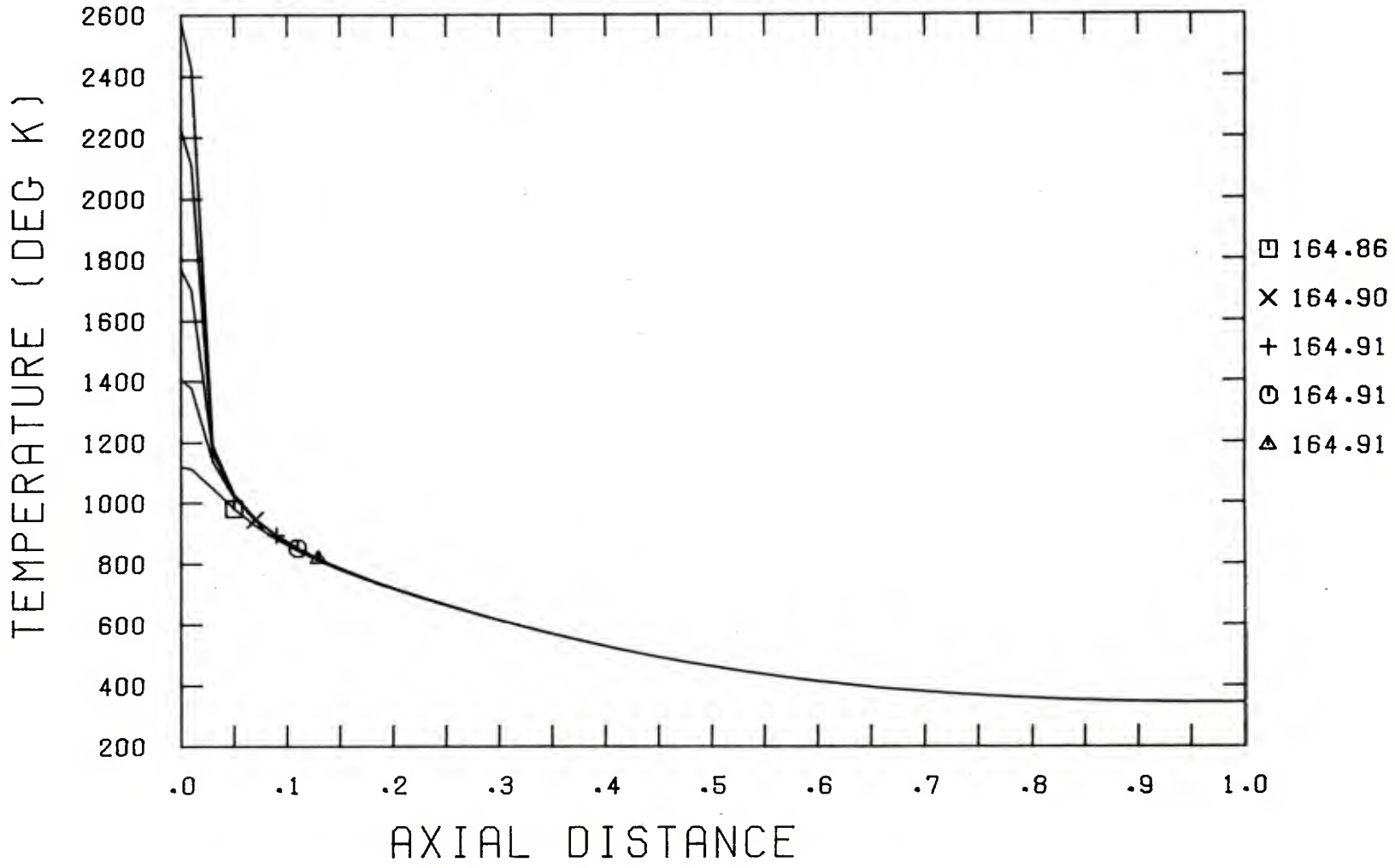

Figure 15. Temperature Distribution for Standard Case (t_{mq}=127.87) Showing Flame Formation

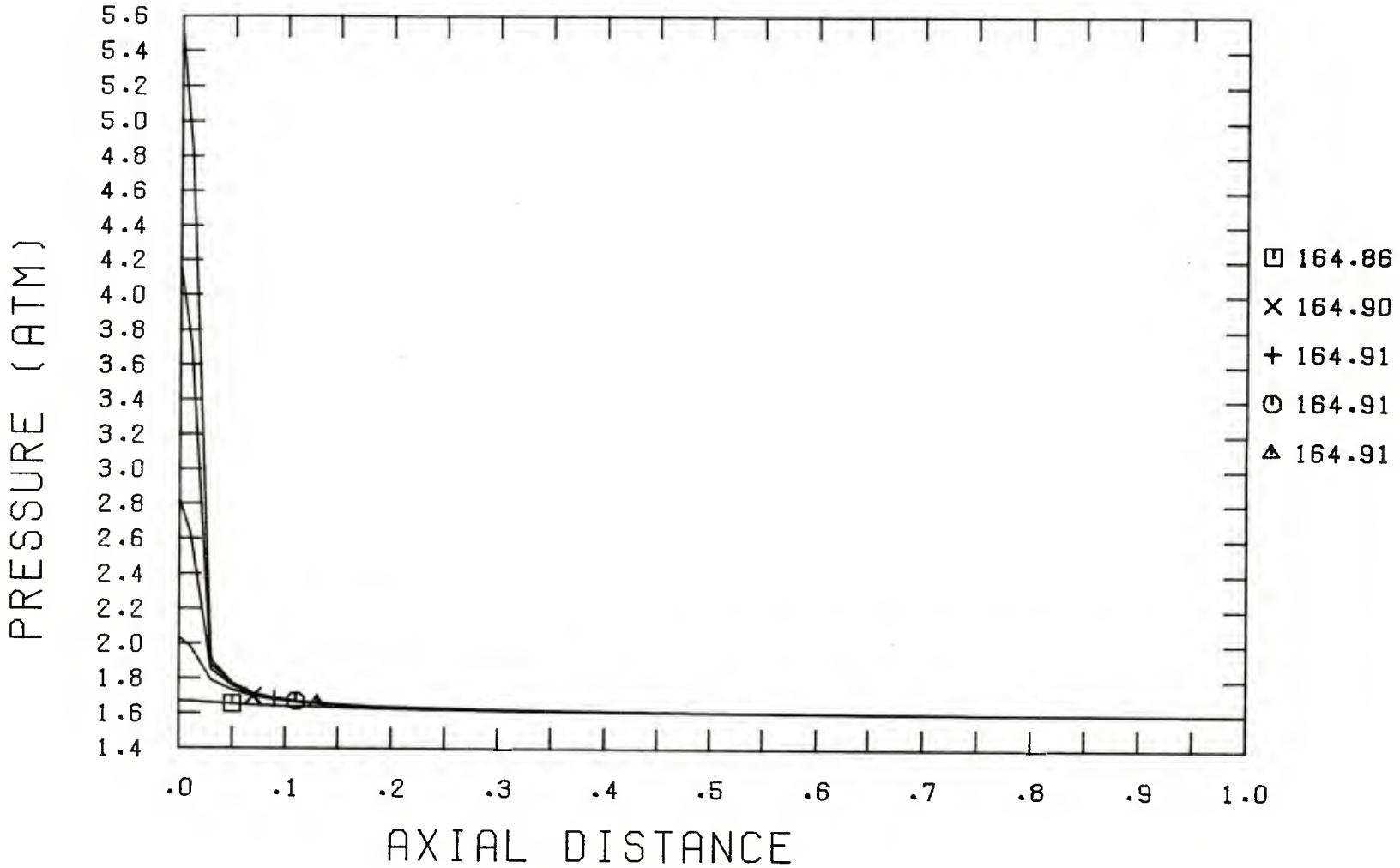

Figure 16. Pressure Distribution for Standard Case (t_{mq}=127.87) Showing Shock Wave Formation

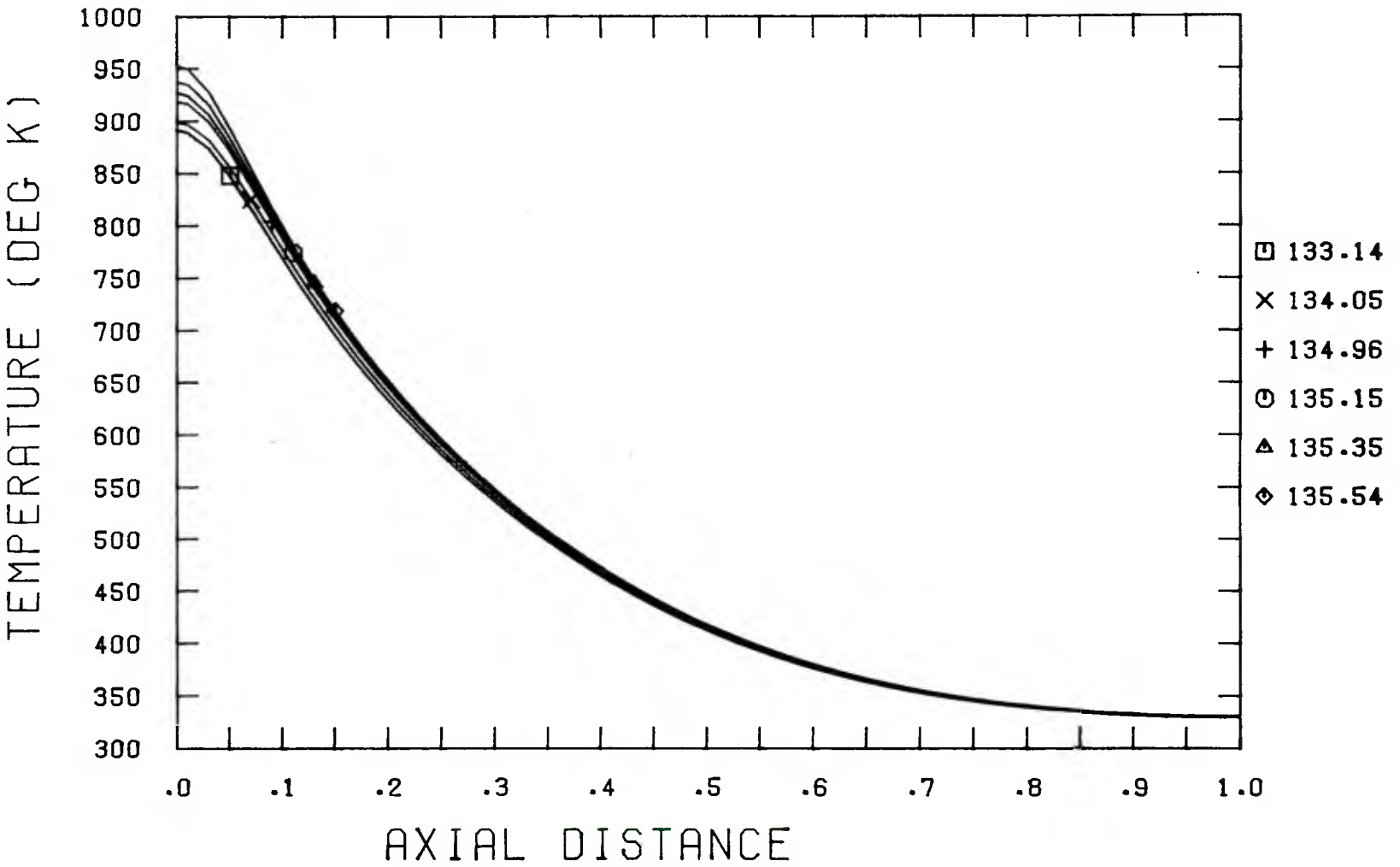

Figure 17a. Temperature Distribution for Standard Case (t_{mq}=128.0) As Runaway Reaction Begins

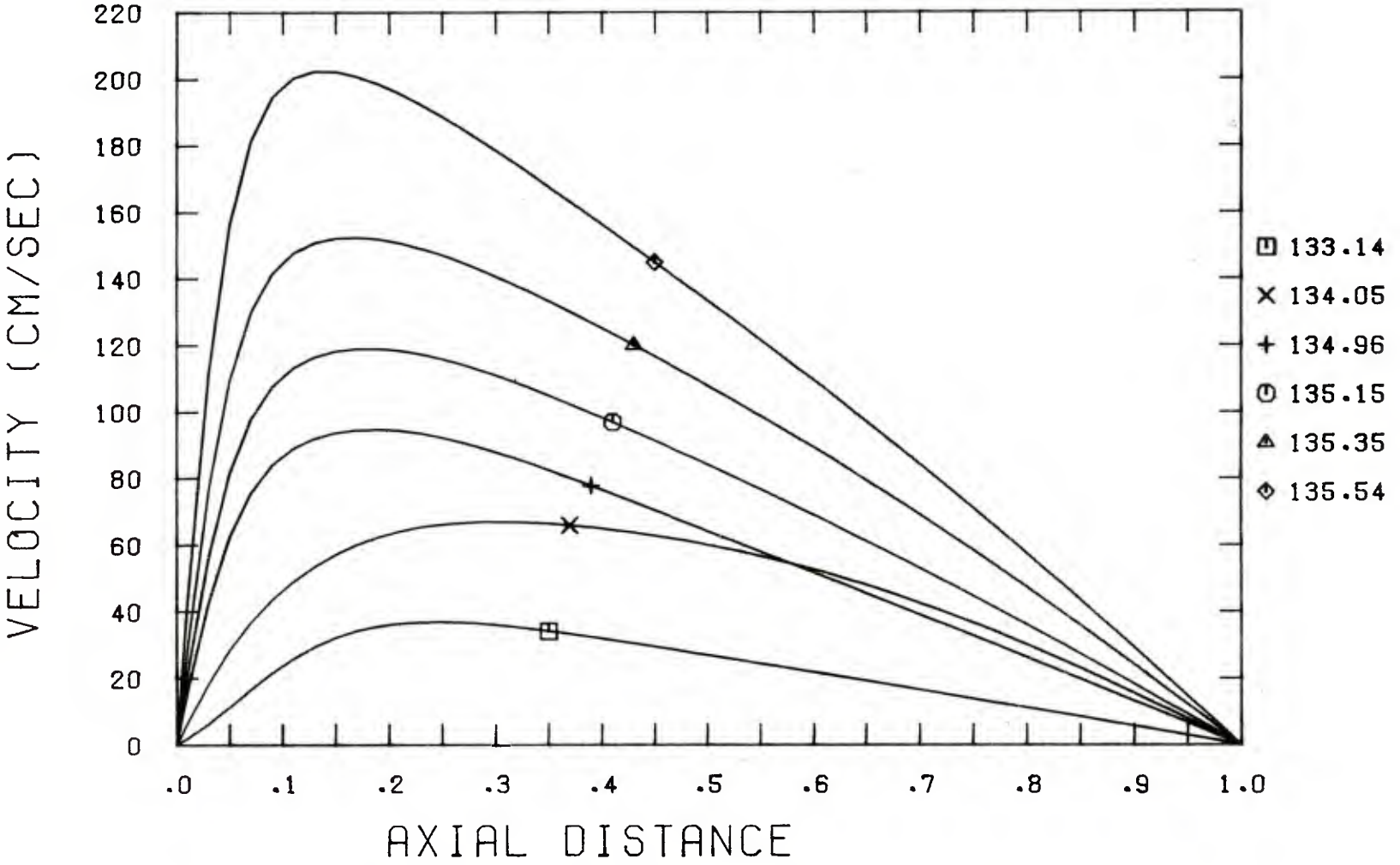

Figure 17b. Velocity Distribution for Standard Case (t_{mq}=128.0) as Runaway Reaction Begins

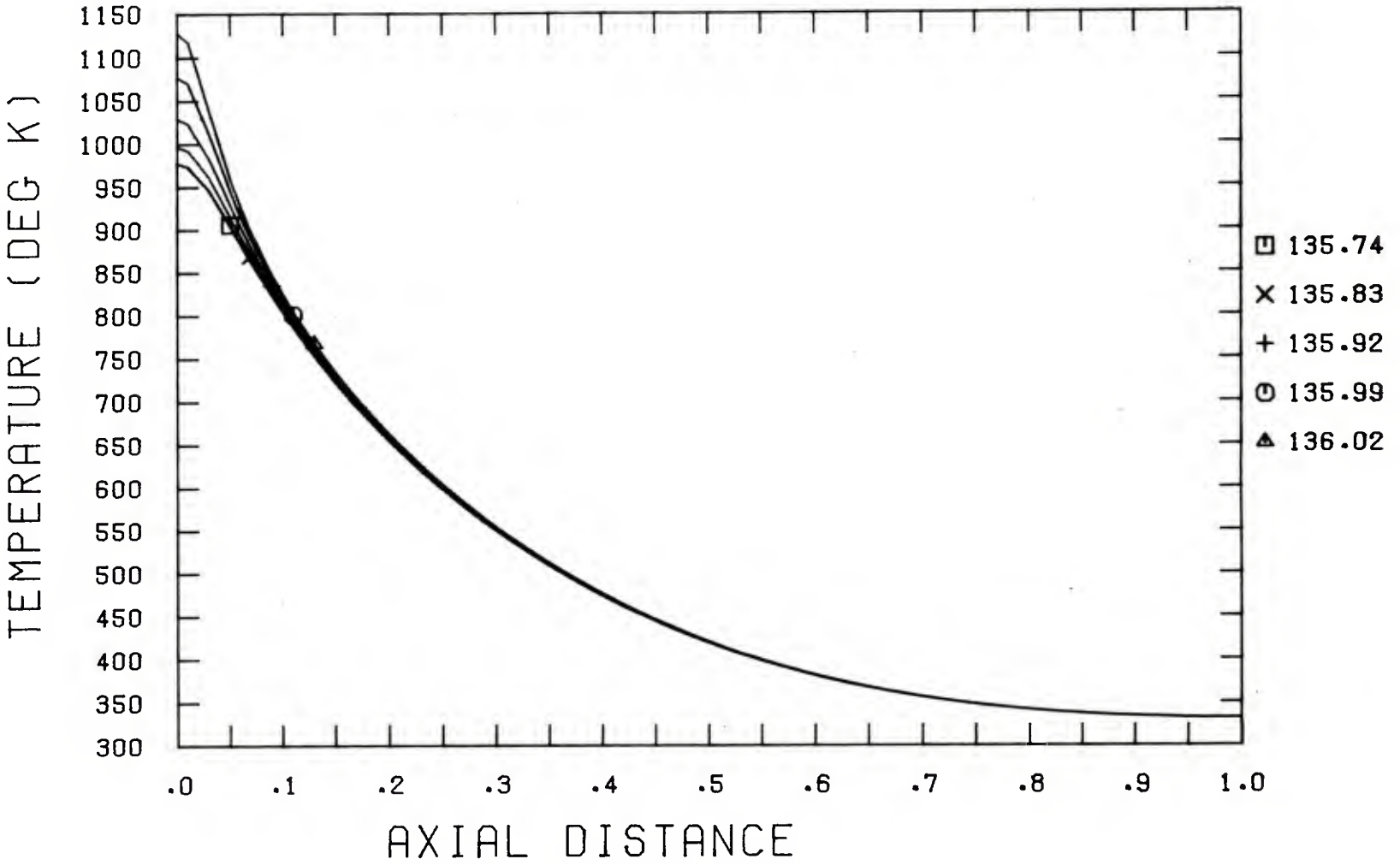

Figure 17c. Temperature Distribution for Standard Case (t_{mq}=128.0) As Runaway Reaction Accelerates

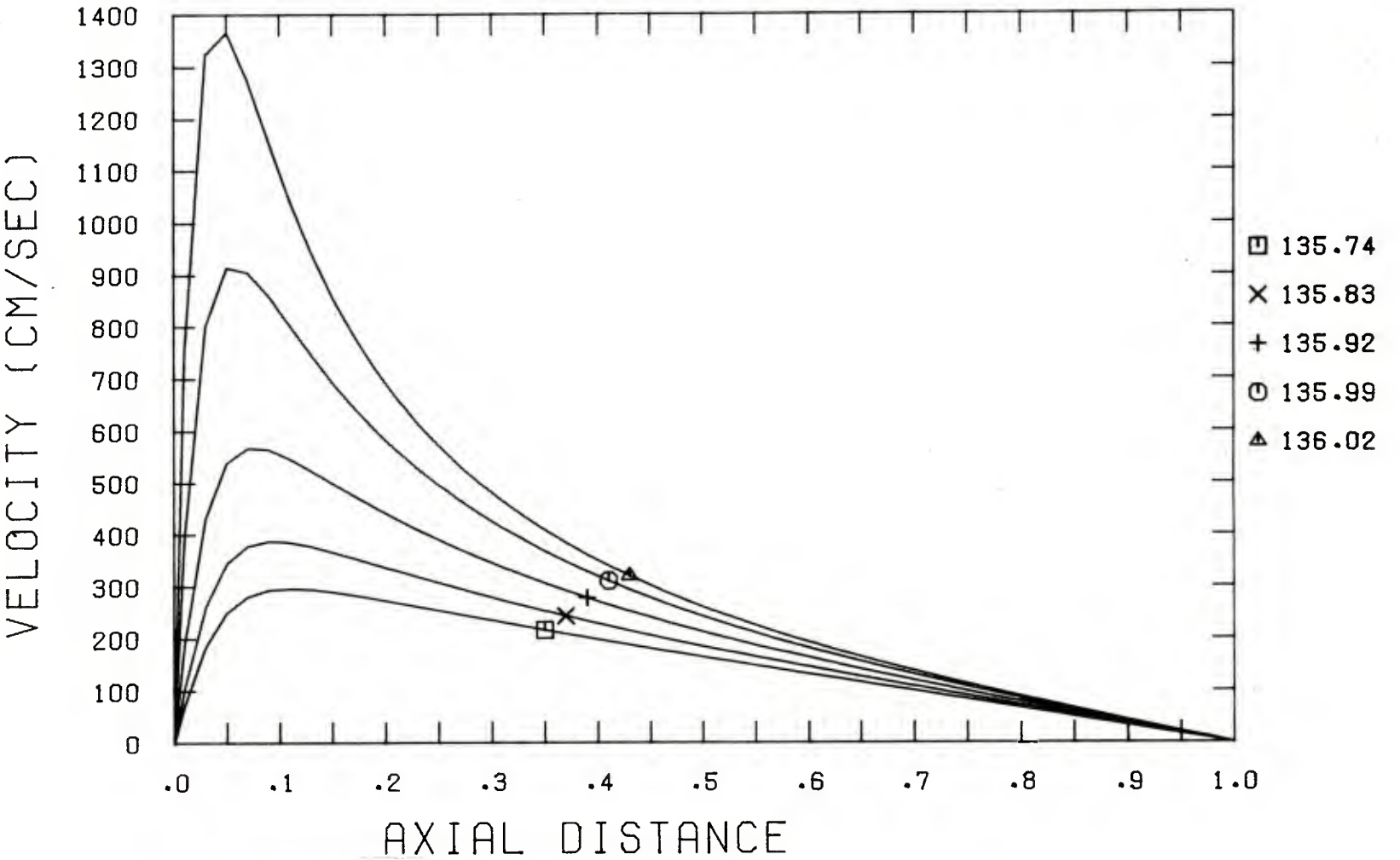

Figure 17d. Velocity Distribution for Standard Case (t_{mq}=128.0) As Runaway Reaction Accelerates

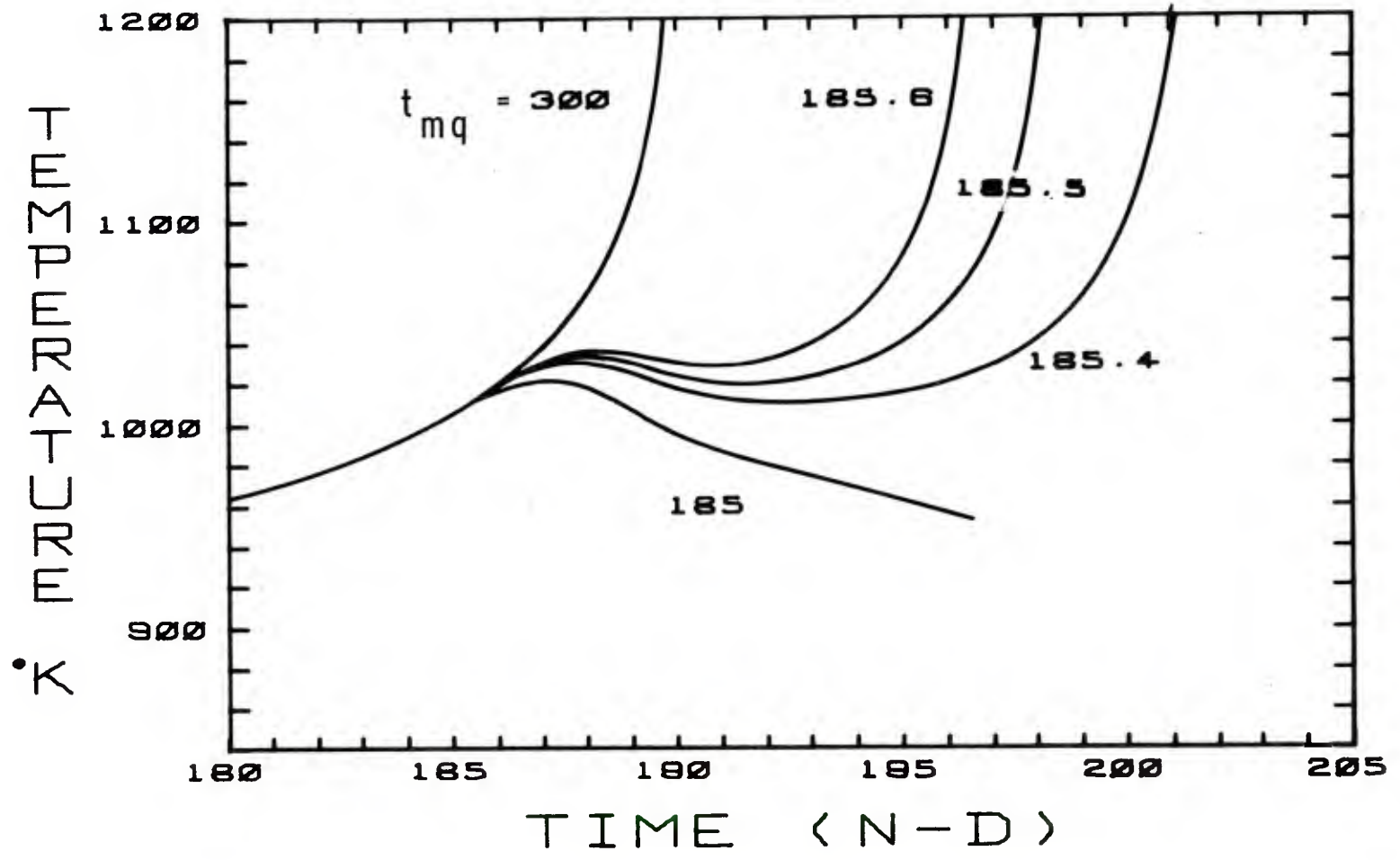

Figure 18. Temperature-Time History At Heated Wall (Varying t_{mq}) For Case CV2

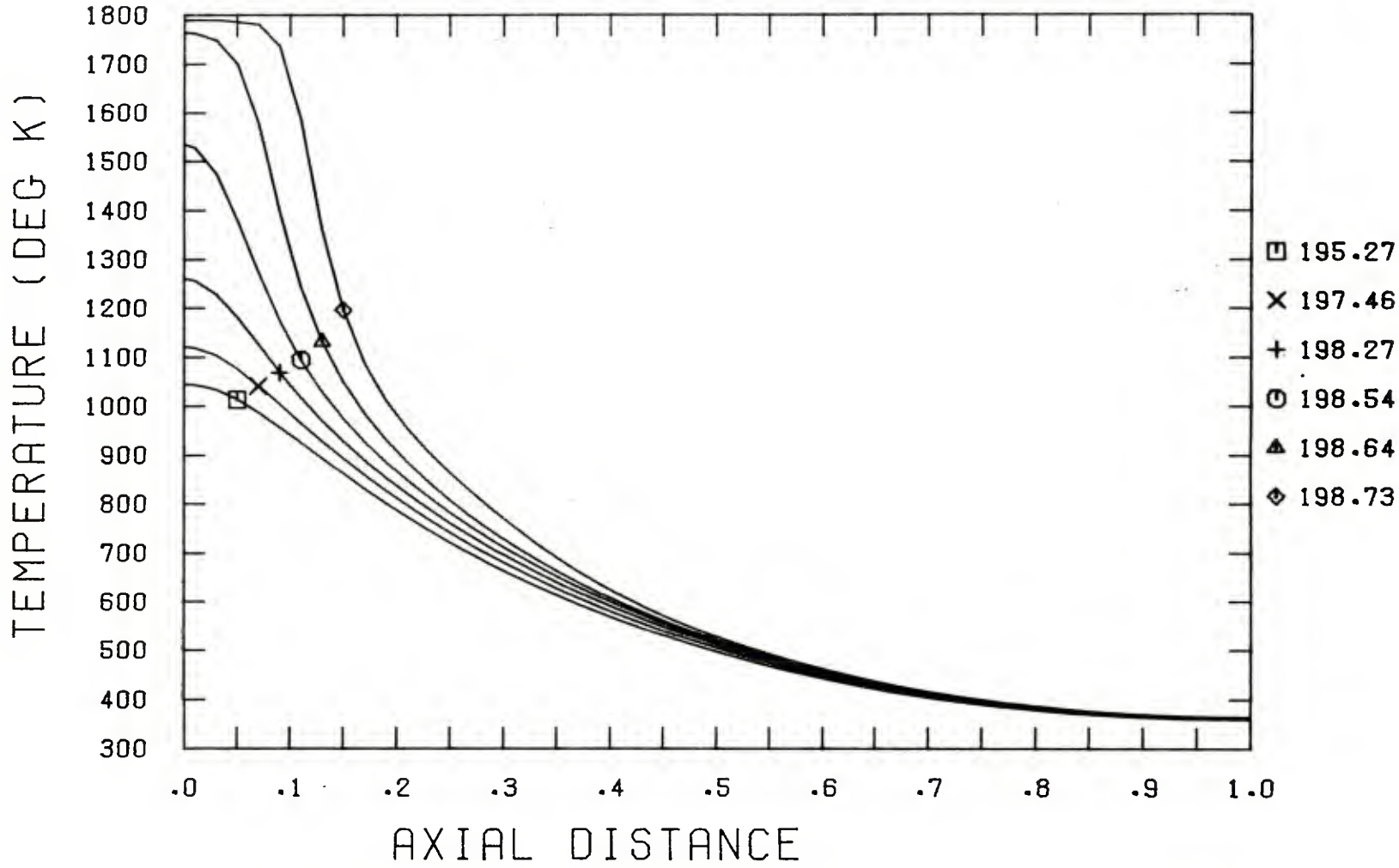

Figure 19. Temperature Distribution for Case CV2 (t_{mq}=185.5) Showing Flame Formation

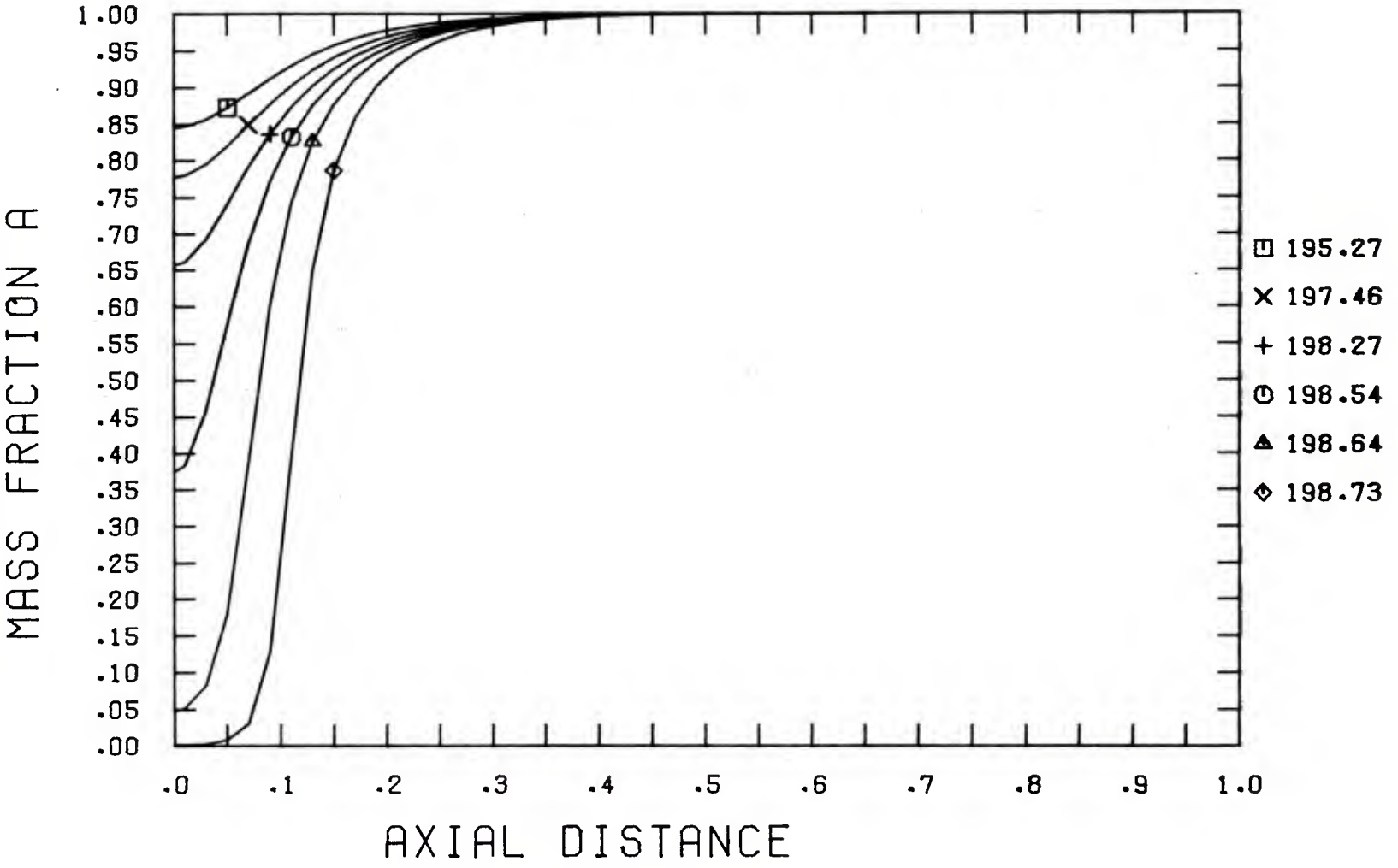

Figure 20. Reactant Mass Fraction Distribution for Case CV2 (t_{mq}=185.5) Showing Flame Formation

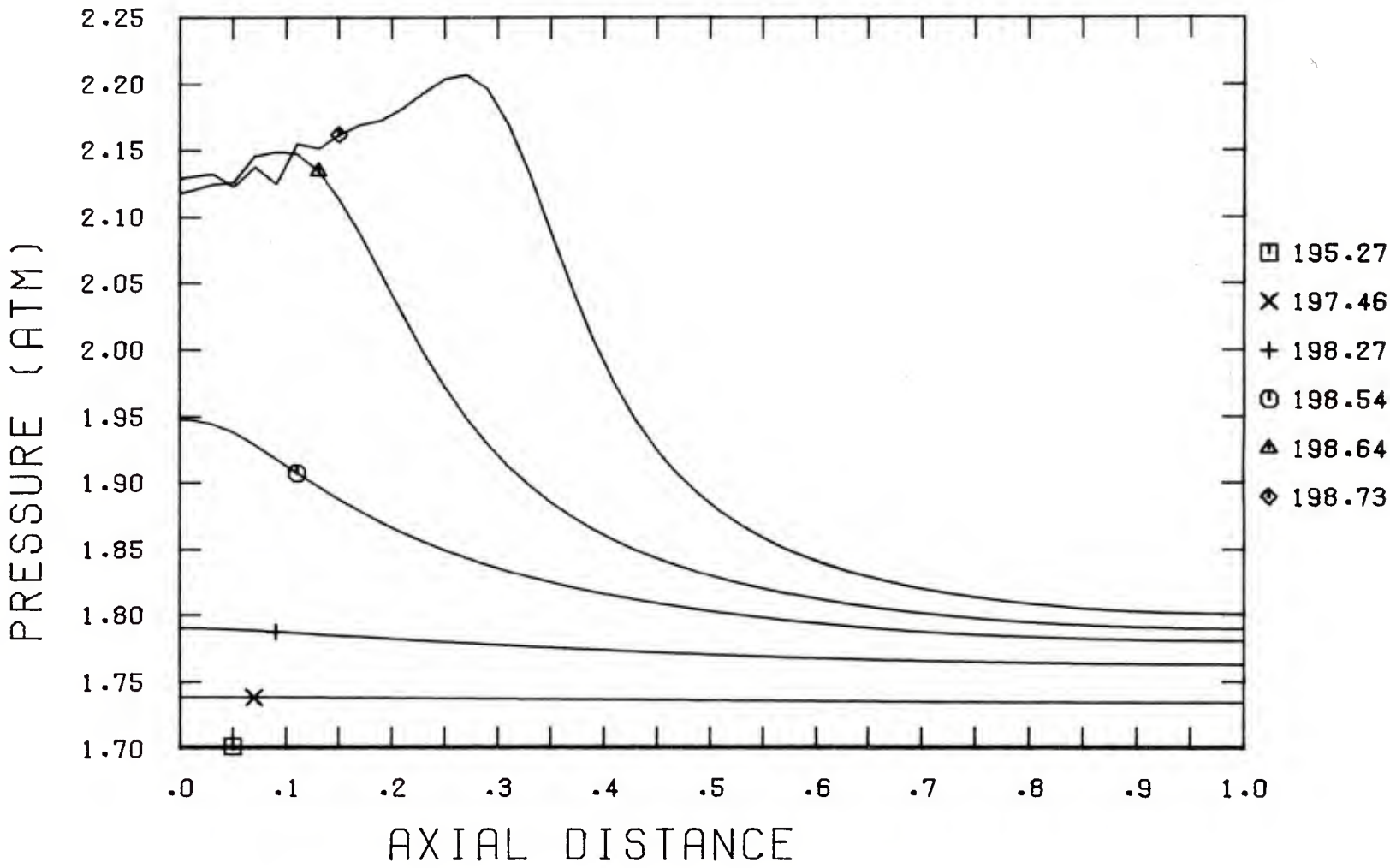

Figure 21. Pressure Distribution for Case CV2 (t_{mq}=185.5)

classical description of a laminar deflagration wave in which the pressure decreases slightly across the combustion front. Of course, a compression wave must precede the subsonic deflagration in order to satisfy the wall boundary condition at z=0. The slight "raggedness" of the predicted pressure in this region is non-physical, and is the direct result of violating the cell Reynolds number limitation discussed earlier. Increased grid point resolution would eliminate the problem.

Correlation of Results

The results obtained in the parametric study for time to ignition are summarized in Table 2. The critical value of ignition time for each case is taken to be the value of t_{mq} which yields the longest hang-fire. The temperature-time history for each case can be found in Appendix A. A better perspective of the sensitivity of ignition time to a change in one of the kinetic parameters can be seen with a simple power law correlation. These correlations are given below:

(a) ignition time vs. activation energy

$$t_{mq} \alpha (E^*)^{2.9}$$

(b) ignition time vs. heat of reaction

$$t_{mq} \alpha (\Delta H^*)^{-.178}$$

(c) ignition time vs. pre-exponential factor

$$t_{mq} \alpha (Z^*)^{-.132}$$

Thus, an increase in activation energy will substantially increase the time to ignition, while an increase in the heat of reaction and/or the pre-exponential factor will decrease the time to ignition.

In ignition studies of all types, the question most frequently addressed concerns the dependence of ignition time on external heat flux. To answer this question for a confined pre-mixed gas, the present investigation conducted a special series of runs based on the standard case. (The results for temperature-time history are included in Appendix B). The constant portion of $q_{wall}(t)$ was varied in small increments over the limited range of 10-25 cal/cm^2-sec. The predictions for t_{mq} at go/no-go as a function of the constant portion of q_{wall} correlated exactly as the power law,

$$t_{mq} \alpha q_{wall}^{-m}, \quad m=1.89$$

An interesting comparison can be made with the results of two different solid propellant ignition theories. Bradley and Williams[11] postulated a heterogeneous reaction between a gas-phase oxidizer and the surface of the solid propellant. Their correlation produces the above result with m=1.86, for the activation energy used in the standard case of this paper. Kashiwagi[3] postulated a two reaction model; the solid fuel pyrolyzes (endothermically) at the surface and then reacts in a gas-phase diffusion flame with the ambient oxidizer. The result of his correlation produces the exponent m=1.9, in the heat flux range quoted above.

All three correlations yield nearly the same value for the exponent. In fact, this value is close to 2.00 which is the value obtained from the well-known solution to the heat conduction equation for an inert solid (e.g., see discussion in Ref. 3). The important implication here is that a plot of ignition time versus external heat flux cannot be used to distinguish the mechanism controlling ignition.

IV. CONCLUSIONS

1. Numerical predictions of the gas-phase ignition sequence seem qualitatively correct. In general, the results show that:

a. A confined premixed gas capable of a single, one-step, irreversible, chemical reaction can sustain a hang-fire ignition, i.e., the runaway reaction occurs many time units after the external heat source (ignition stimulus) is terminated.

b. A hang-fire ignition forms the boundary separating "go" and "no-go".

c. The acoustic response of the chamber plays a definite role in the ignition of a confined reactive gas.

d. Successful ignition of the confined premixed gas leads to a thin flame zone, assuming that all transport processes are laminar and that the controlling chemical reaction is a single, one-step, irreversible decomposition. When the exothermic heat of reaction is sufficiently large, the numerical solution predicts the formation of a detonation wave.

---

[11] *Bradley, H. H., Jr., and Williams, F. A., "Theory of Radiant and Hypergolic Ignition of Solid Propellants", Comb. Sci. Tech., Vol. 2, pp 41-52 (1970).*

2. Correlations of the numerical results were established to show that:

a. An increase in activation energy (E^*) will substantially increase the time to ignition.

b. An increase in the exothermic heat of reaction (ΔH^*) will decrease the time to ignition.

c. An increase in the pre-exponential factor (Z^*) will decrease the time to ignition.

3. The dependence of ignition time on external heat flux cannot be used to distinguish a simple premixed gas-phase reaction from other mechanisms which may control ignition.

V. ACKNOWLEDGMENT

The author gratefully acknowledges the substantial contribution of R. D. Anderson who executed the computer program and constructed the CALCOMP plots.

REFERENCES

1. Kooker, D. E., and Nelson, C. W., "Numerical Solution of Three Solid Propellant Combustion Models During a Gun Pressure Transient", BRL Report No. 1953 (AD No. A035250), Ballistic Research Lab, Aberdeen Proving Ground, MD, January 1977 (see also 12th JANNAF Combustion Meeting, Newport, RI, CPIA Publication 273, pp 173-197, Dec 75).

2. Hermance, C. W., and Kumar, R. K., "Gas Phase Ignition Theory for Homogeneous Propellants Under Shock Tube Conditions", AIAA J., Vol 8, No. 9, pp 1551-1558 (Sep 70).

3. Kashiwagi, T., "A Radiative Ignition Model of a Solid Fuel," Comb. Sci. Tech., Vol. 8, pp 225-236 (1974).

4. Bradley, H. H., Jr., "A Unified Theory of Solid Propellant Ignition, Part 1, Development of Mathematical Model," NWC TP5618 (Aug 74).

5. Kindelan, M., and Williams, F. A., "Radiant Ignition of a Combustible Solid with Gas-Phase Exothermicity," Acta Astronautica, Vol. 2, No. 11/12 (Nov/Dec 75).

6. Rivard, W. C., Farmer, O. A., and Butler, T. D., "RICE: A Computer Program for Multicomponent Chemically Reactive Flows at All Speeds," LA-5812, Los Alamos Scientific Laboratory, Los Alamos, NM, Mar 75.

7. Kothari, A. P., Anderson, J. D., Jr., and Jones, E., "Navier-Stokes Solutions for Chemical Laser Flows", AIAA J., Vol. 15, No. 1, pp 92-100 (Jan 77).

8. Edelman, R. B., Fortune, O. F., and Weilerstein, G., "An Analytical and Experimental Investigation of Gravity Effects Upon Laminar Gas Jet-Diffusion Flames", 14th Symposium (International) on Combustion, Aug 72, Penn State University, pp 399-412.

9. Merzhanov, A. G., and Averson, A. E., "The Present State of the Thermal Ignition Theory: An Invited Review," Comb. Flame, Vol. 16, pp 89-124 (1971).

10. Bradley, H. H. Jr., "Theory of Ignition of a Reactive Solid by Constant Energy Flux," Comb. Sci. Tech., Vol. 2, pp 11-20 (1970).

11. Bradley, H. H. Jr., and Williams, F. A., "Theory of Radiant and Hypergolic Ignition of Solid Propellants", Comb. Sci. Tech., Vol. 2, pp 41-52 (1970).

APPENDIX A

Ignition Results for Parametric Study

This appendix contains the numerical results obtained near the critical ignition point for each case considered in the parametric study (for the Standard Case, see Fig. 14, page 31). Each of the figures to follow pertains to a single case and displays multiple curves of gas temperature adjacent to the heated wall (z=0) as a function of time; the only parameter varied is the cut-off time, t_{mq}, of the external heat flux. The constant portion of the external heat flux, $q_{wall}(t)$, is held constant at 10 cal/cm^2-sec. The value of t_{mq} which yields the longest hang-fire is taken as the "time to ignition" and was recorded in Table 2 on page 20.

Case	$\hat{E}^*$ $\frac{kcal}{mole}$	Z^* sec^{-1}	ΔH^* (exothermic) $\frac{kcal}{mole}$
Std.	35	10^{13}	35
CV 1	35	10^{12}	35
CV 2	35	10^{12}	25
CV 3	35	10^{12}	30
CV 4	35	10^{13}	30
CV 5	35	10^{14}	30
CV 6	30	10^{12}	30
CV 7	30	10^{13}	30

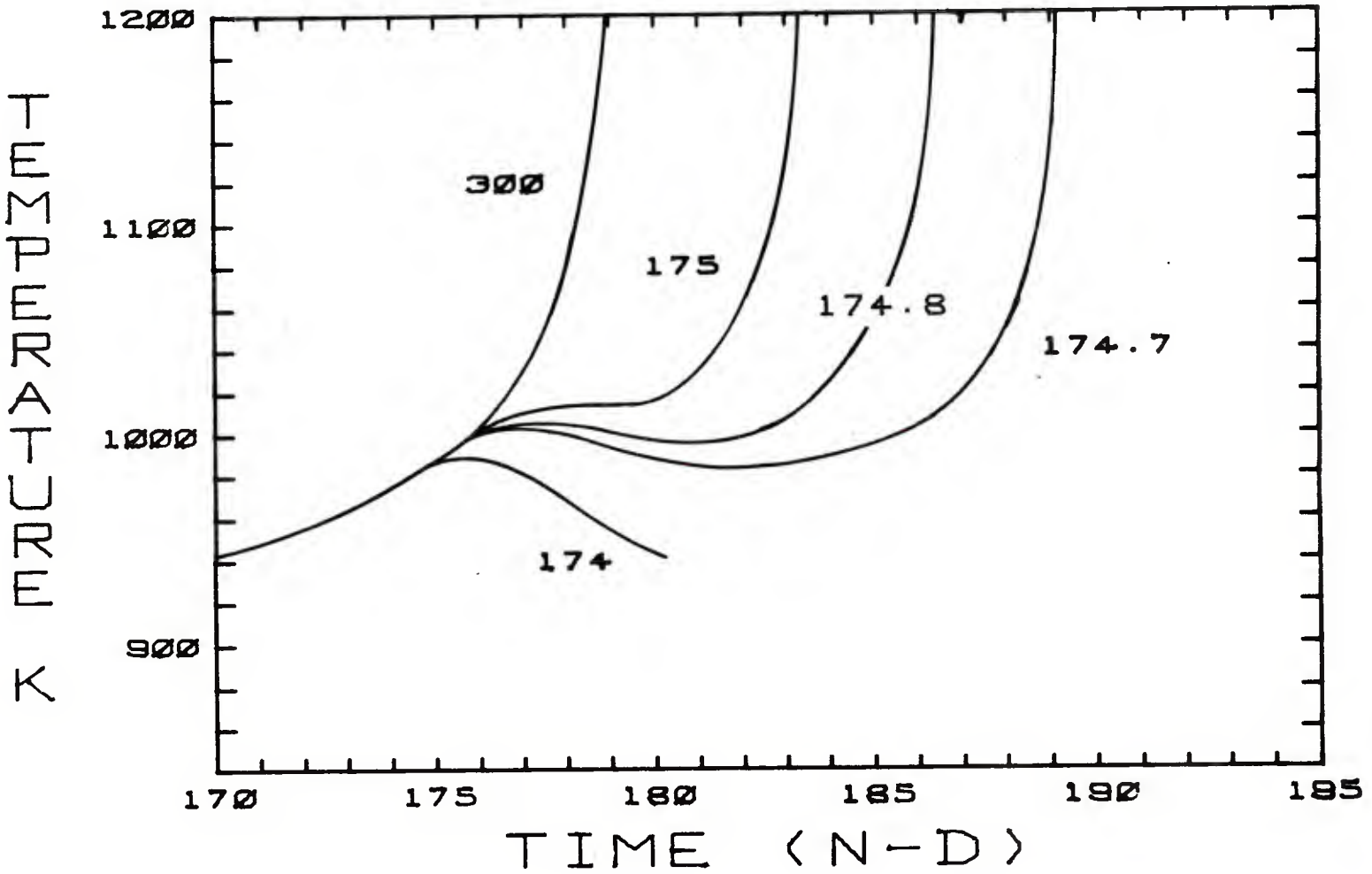

Figure A-1 Temperature-Time History at Heated Wall (Varying t_{mq}) for Case CV 1

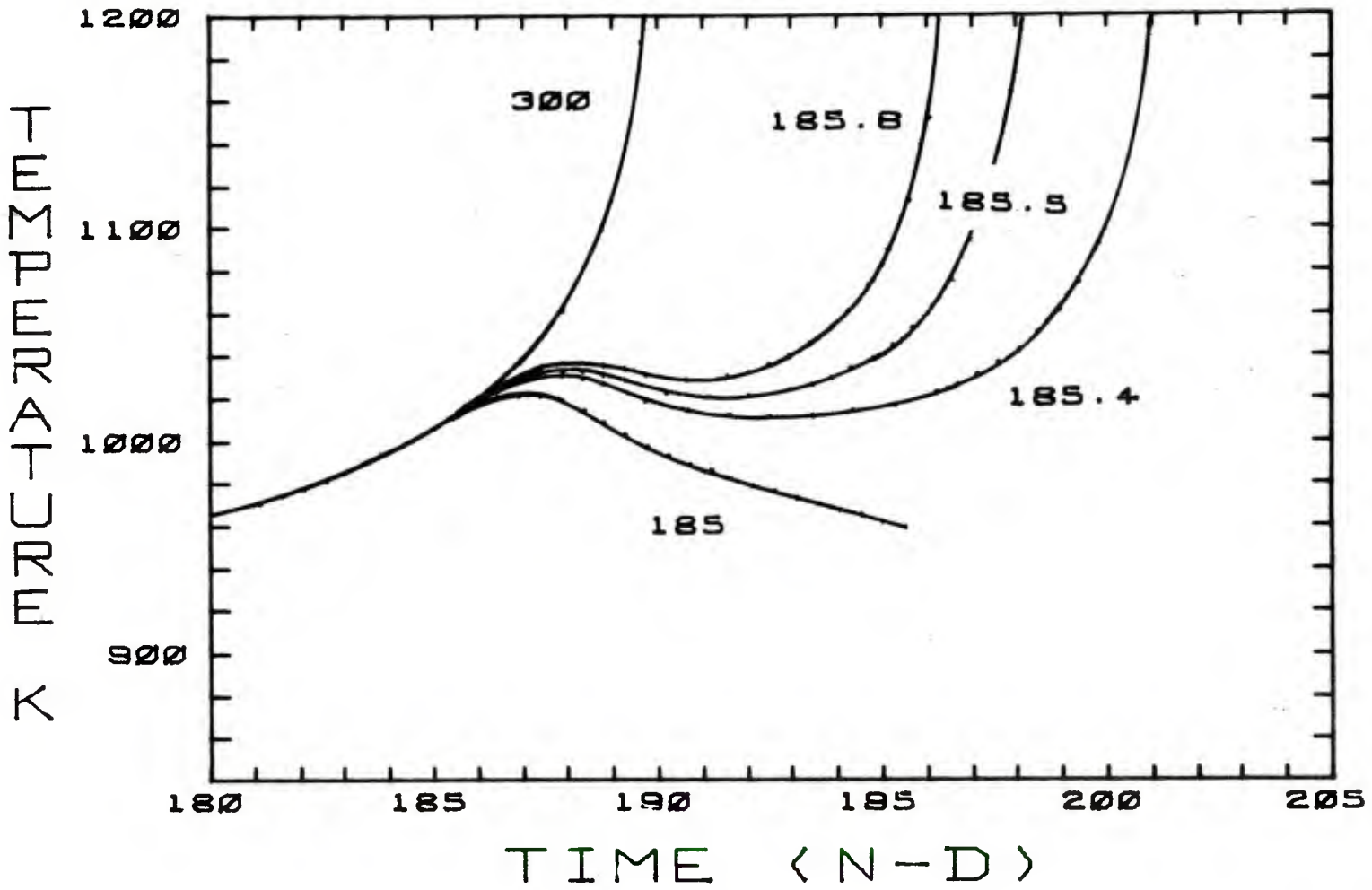

Figure A-2 Temperature-Time History at Heated Wall (Varying t_{mq}) for Case CV 2

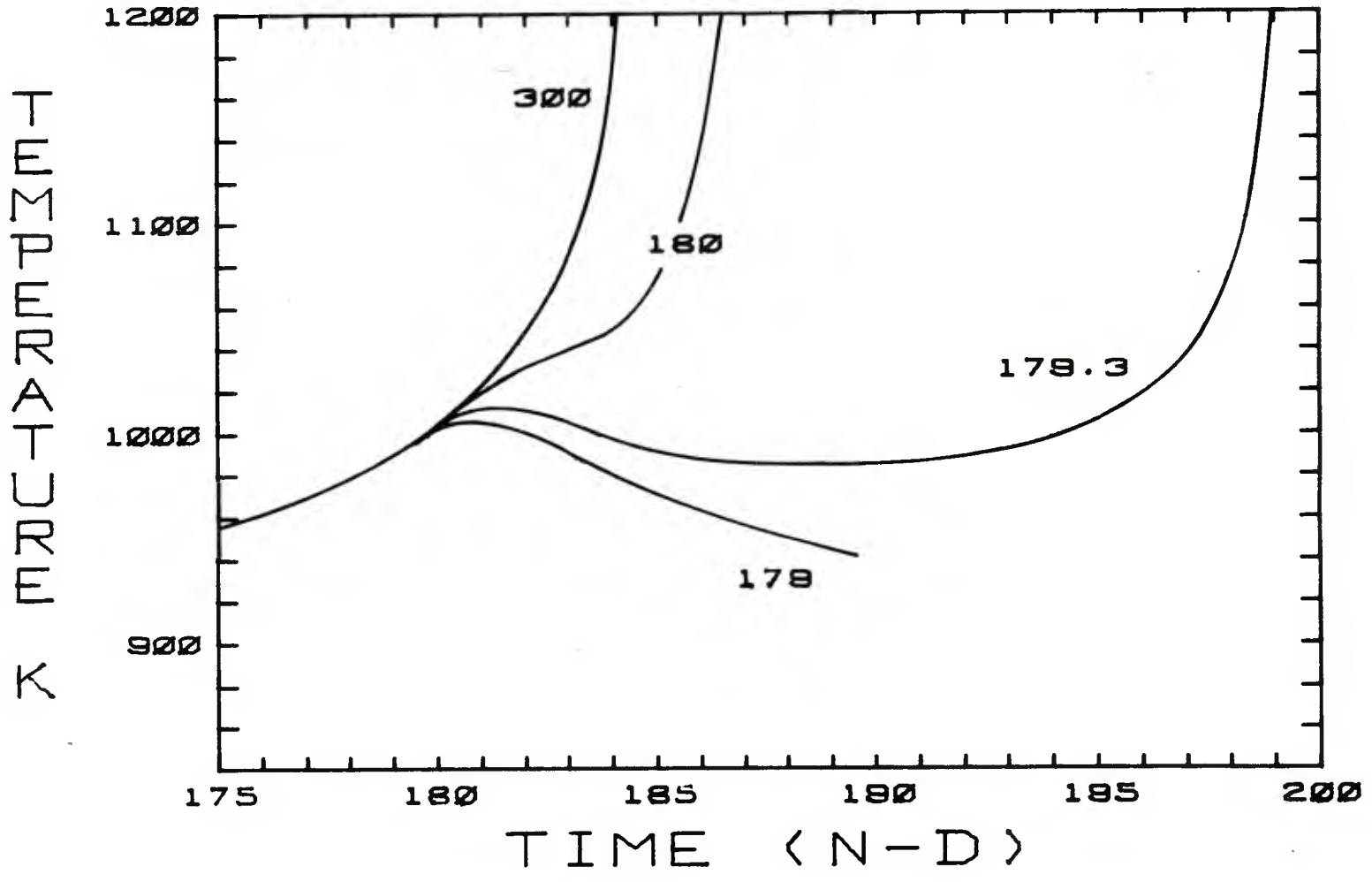

Figure A-3 Temperature-Time History at Heated Wall (Varying t_{mq}) for Case CV 3

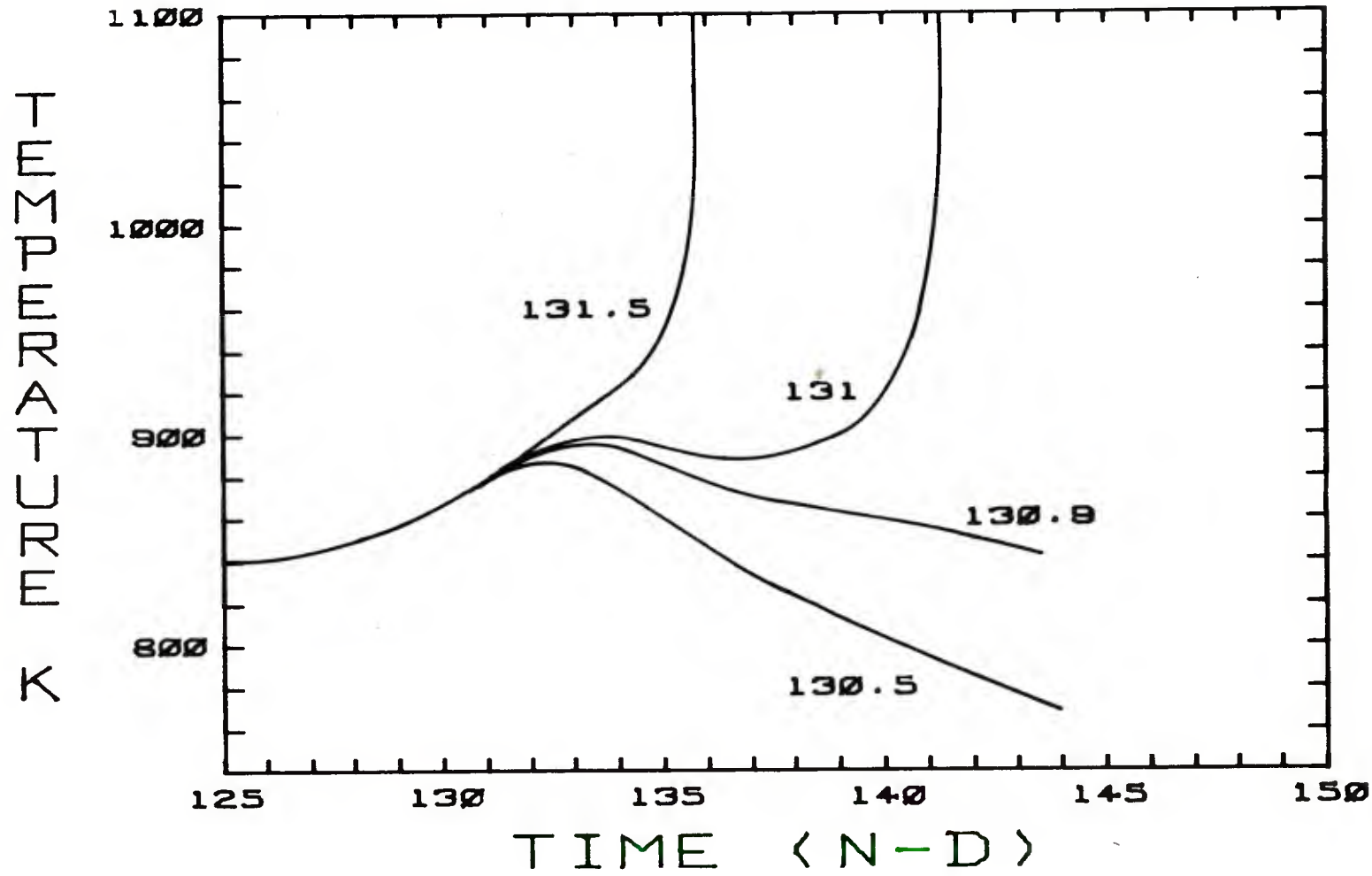

Figure A-4 Temperature-Time History at Heated Wall (Varying t_{mq}) for Case CV 4

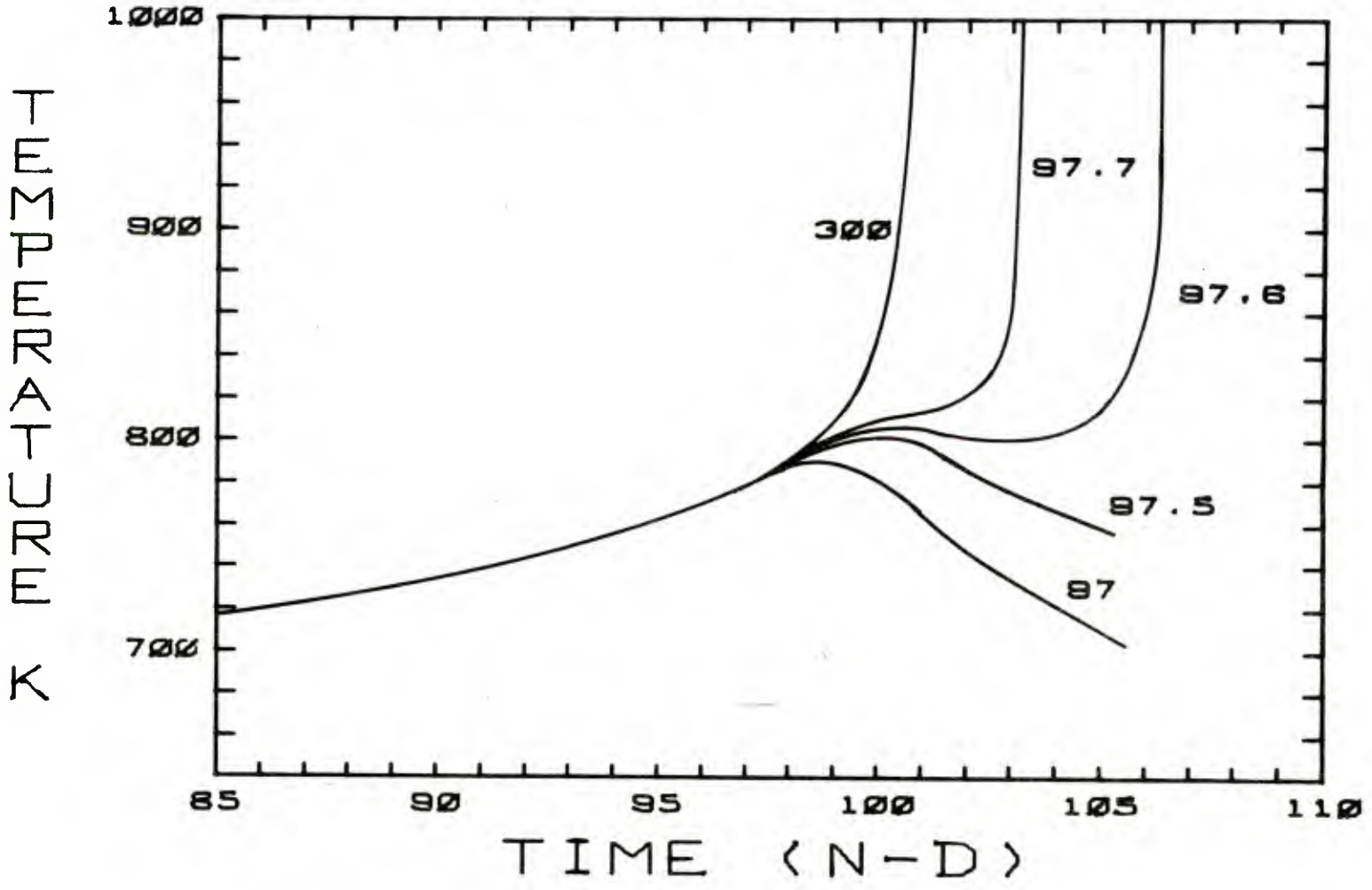

Figure A-5 Temperature-Time History at Heated Wall (Varying t_{mq}) for Case CV 5

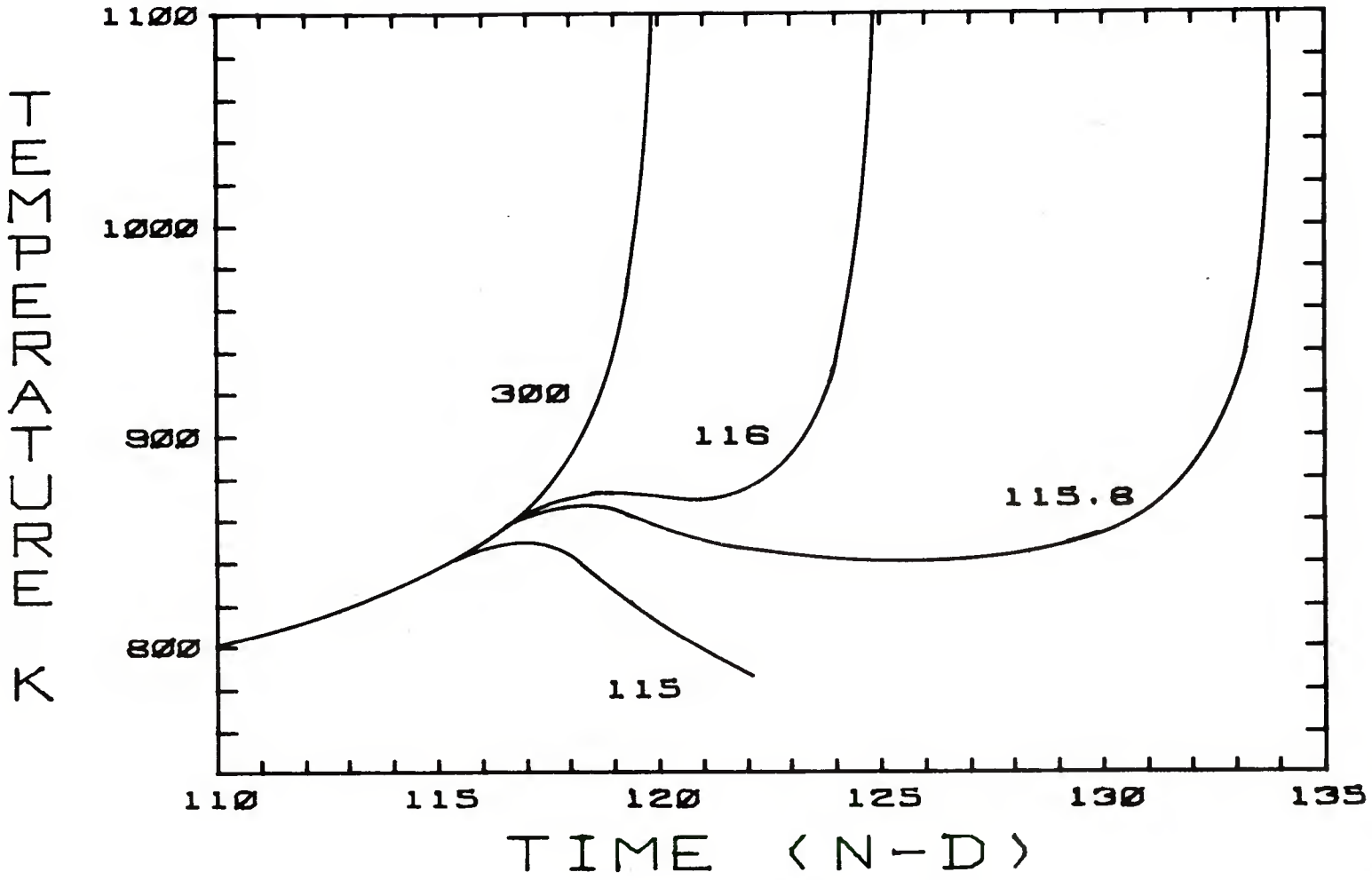

Figure A-6 Temperature-Time History at Heated Wall (Varying t_{mq}) for Case CV 6

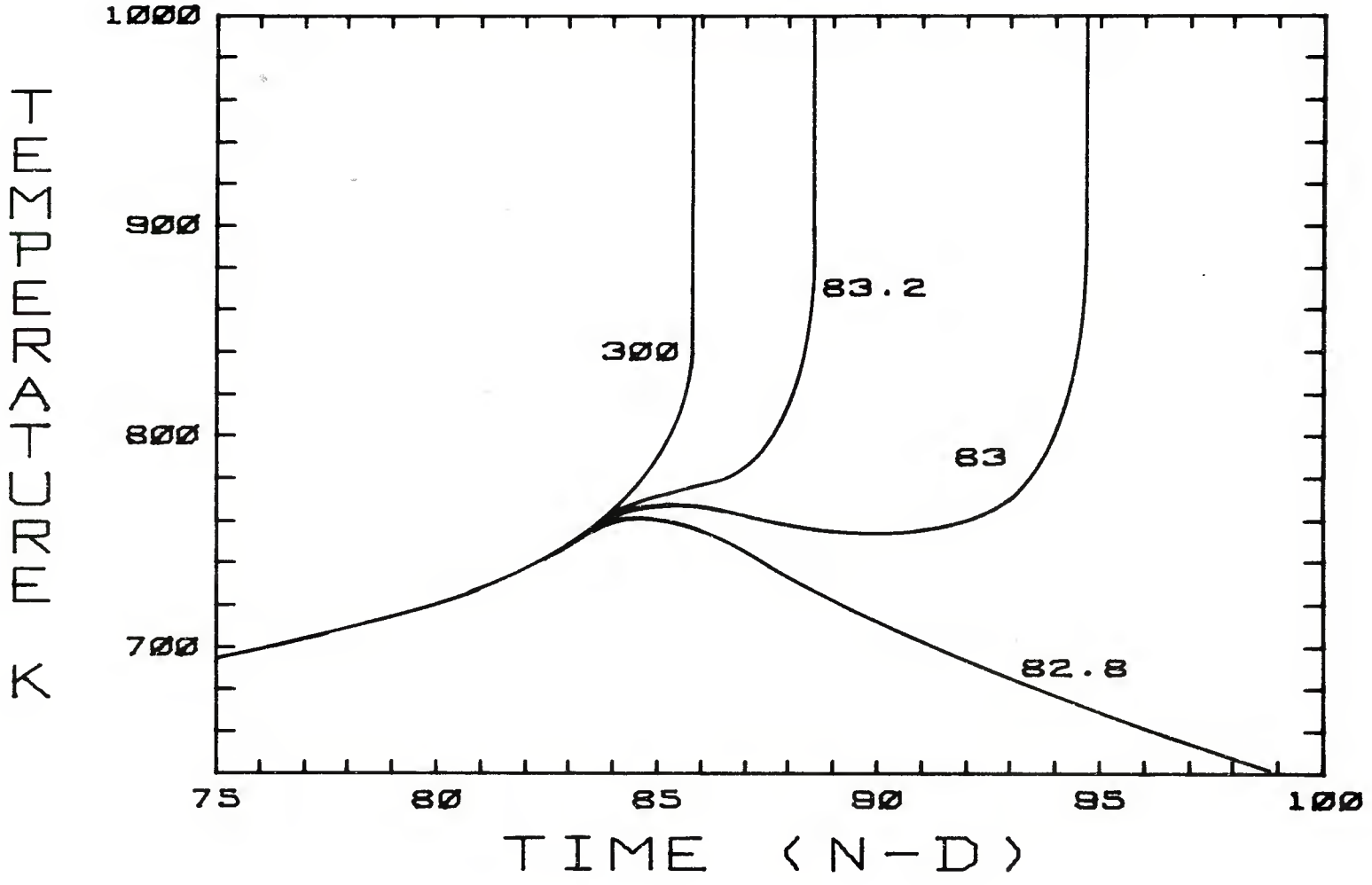

Figure A-7 Temperature-Time History at Heated Wall (Varying t_{mq}) for Case CV 7

APPENDIX B

Ignition Results for Variable External Heat Flux

This appendix contains the numerical results obtained near the critical ignition point for the study of ignition time dependence on external heat flux level. All of the figures to follow are based on the set of parameters denoted as the Standard Case. Each figure corresponds to a particular value for the constant portion of the external heat flux, $q_{wall}(t)$ (see Fig. 3, page 16). The value of this constant portion is varied over the range 10-25 cal/cm^2-sec. Similar to Appendix A, the results are displayed as multiple curves of gas temperature adjacent to the heated wall (z=0) as a function of time; the only parameter varied is the cut-off time, t_{mq}, of the external heat flux. The value of t_{mq} which yields the longest hang-fire is taken as the "time to ignition" and was used to obtain the correlation,

$$t_{mq} \propto q_{wall_o}^{-1.89} .$$

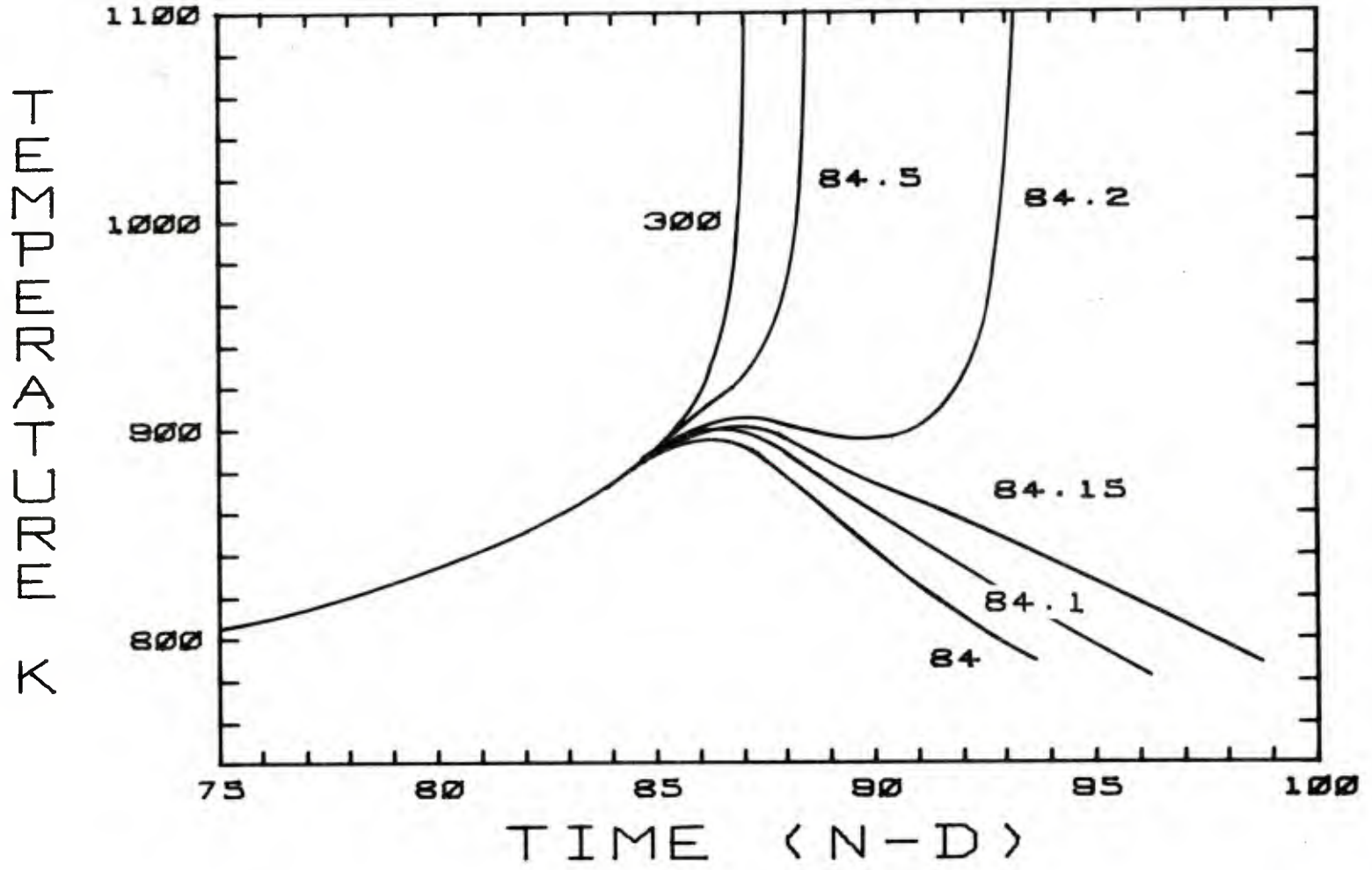

Figure B-1 Temperature-Time History at Heated Wall (Varying t_{mq}) for q_{wall_o} = 12.5 cal/cm^2-sec

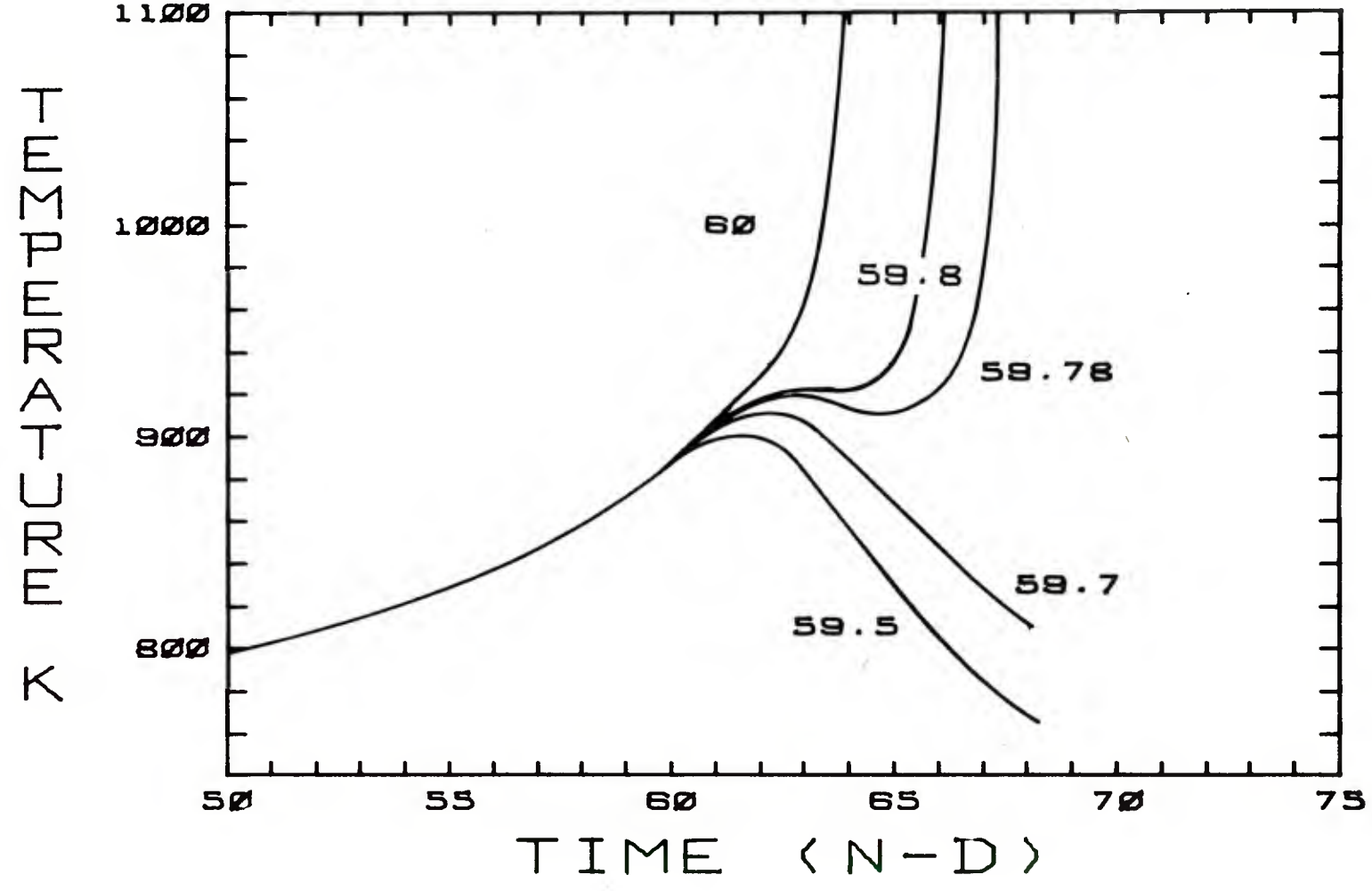

Figure B-2 Temperature-Time History at Heated Wall (Varying t_{mq}) for q_{wall_o} = 15.0 cal/cm^2-sec

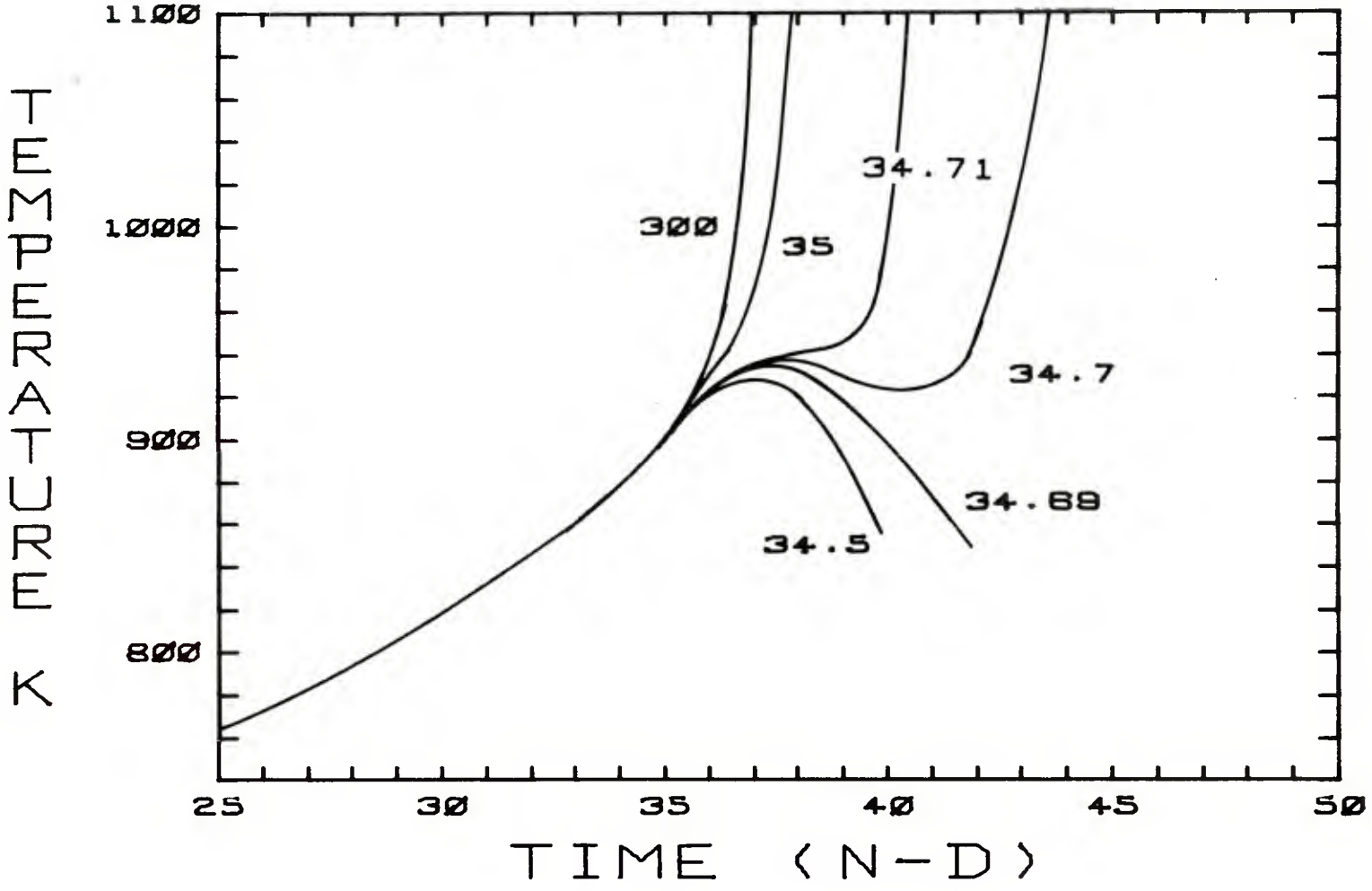

Figure B-3 Temperature-Time History at Heated Wall (Varying t_{mq}) for q_{wall_o} = 20.0 cal/cm^2-sec

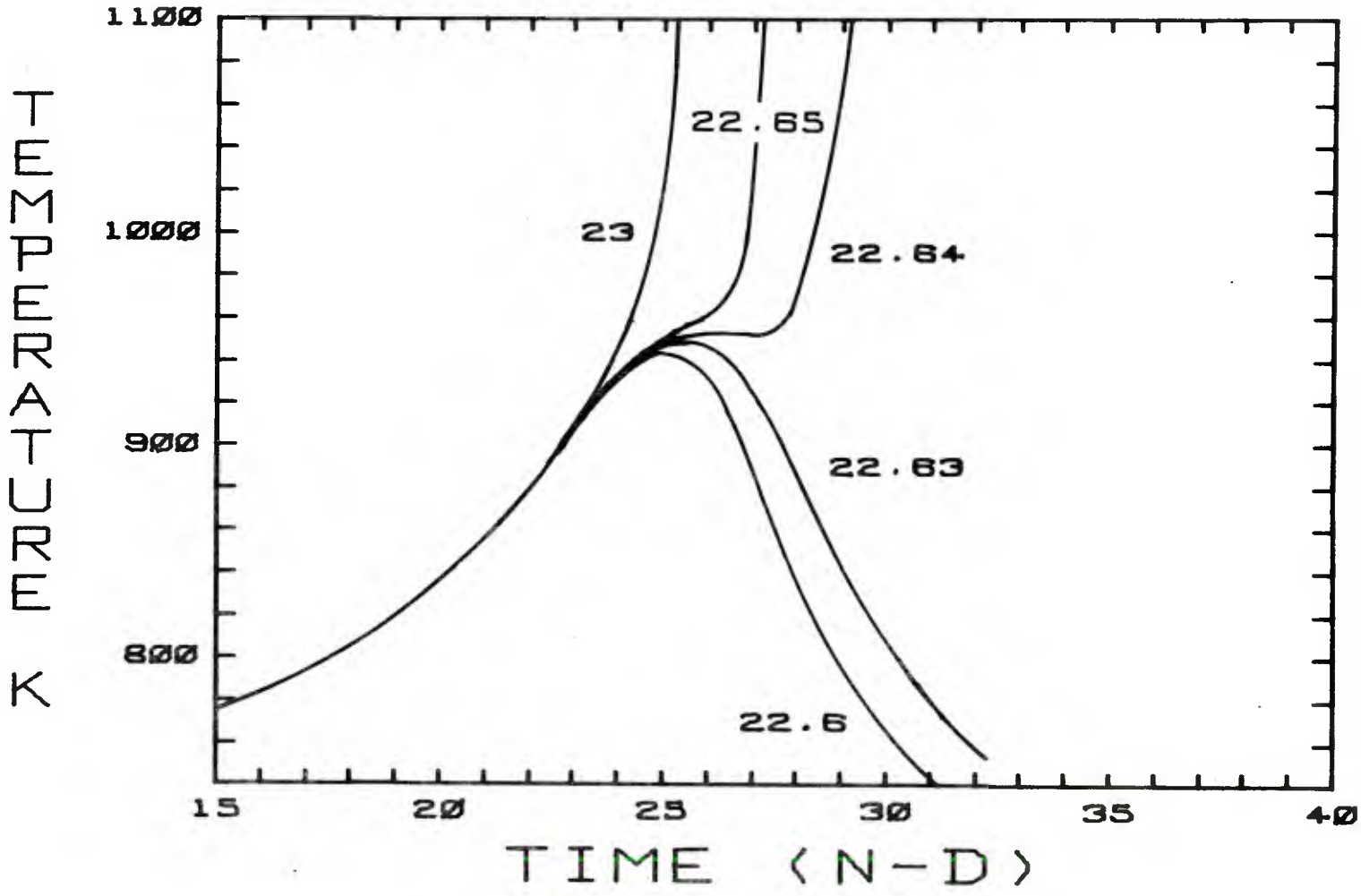

Figure B-4 Temperature-Time History at Heated Wall (Varying t_{mq}) for q_{wall_o} = 25.0 cal/cm^2-sec

DISTRIBUTION LIST

No. of Copies	Organization
12	Commander Defense Documentation Center ATTN: DCC-TCA Cameron Station Alexandria, VA 22314
1	Director Defense Advanced Research Projects Agency ATTN: C. R. Lehner 1400 Wilson Boulevard Arlington, VA 22209
2	Director Institute for Defense Analyses ATTN: Dr. H. Wolfhard R. T. Oliver 400 Army-Navy Drive Arlington, VA 22202
1	Commander US Army Materiel Development and Readiness Command ATTN: DRCDMA-ST 5001 Eisenhower Avenue Alexandria, VA 22333
1	Commander US Army Aviation Research and Development Command ATTN: DRSAV-E 12th and Spruce Streets St. Louis, MO 63166
1	Director US Army Air Mobility Research and Development Laboratory Ames Research Center Moffett Field, CA 94035
1	Commander US Army Electronics Command ATTN: DRSEL-RD Ft. Monmouth, NJ 07703
1	Commander US Army Missile Research and Development Command ATTN: DRDMI-R Redstone Arsenal, AL 35809
1	Commander US Army Tank Automotive Development Command ATTN: DRDTA-RWL Warren, MI 48090
2	Commander US Army Mobility Equipment Research & Development Command ATTN: Tech Doc Ctr, Bldg 315 DRSME-RZT Ft. Belvoir, VA 22060
1	Commander US Army Armament Materiel Readiness Command ATTN: DRSAR-LEP-L, Tech Lib Rock Island, IL 61299
4	Commander US Army Armament Research and Development Command ATTN: C. Lenchitz J. Lannon D. Downs H. Fair Dover, NJ 07801
1	Commander US Army White Sands Missile Range ATTN: STEWS-VT WSMR, NM 88002
1	Commander US Army Watervliet Arsenal ATTN: R. Thierry/Code SARWV-RD Watervliet, NY 12189

DISTRIBUTION LIST

No. of Copies	Organization
1	Commander US Army Materials and Mechanics Research Center ATTN: DRXMR-ATL Watertown, MA 02172
1	Commander US Army Natick Research and Development Command ATTN: DRXRE, Dr. D. Sieling Natick, MA 01762
1	Director US Army TRADOC Systems Analysis Activity ATTN: ATAA-SL, Tech Lib WSMR, NM 88002
1	Commander US Army Research Office ATTN: Tech Lib P.O. Box 12211 Rsch Triangle Park, NC 27706
1	Chief of Naval Research ATTN: Code 473 800 N. Quincy Street Arlington, VA 22217
1	Commander US Naval Sea Systems Cmd ATTN: J. W. Murrin (NAVSEA-0331) National Center Bldg 2, Rm 6E08 Washington, DC 20360
2	Commander US Naval Surface Weapons Ctr White Oak Laboratory ATTN: S. J. Jacobs R. R. Bernecker, R13 Silver Spring, MD 20910
1	Commander US Naval Surface Weapons Center ATTN: Library Br, DX-21 Dahlgren, VA 22448
1	Commander US Naval Underwater Systems Center Energy Conversion Department ATTN: R. S. Lazar/Code 5B331 Newport, RI 02840
2	Commander US Naval Weapons Center ATTN: Dr. R. Derr Mr. H. Bradley China Lake, CA 93555
1	Commander US Naval Research Laboratory ATTN: Code 6180 Washington, DC 20375
3	Superintendent US Naval Postgraduate School ATTN: Tech Lib Dr. David Netzer Dr. Allen Fuhs Monterey, CA 93940
3	Commander US Naval Ordnance Station ATTN: S. E. Mitchell C. B. Dale Tech Lib Indian Head, MD 20640
2	AFOSR ATTN: J. F. Masi Dr. B. T. Wolfson Bolling AFB, DC 20332

DISTRIBUTION LIST

No. of Copies	Organization
2	AFRPL (DYSC) ATTN: Dr. D. George Mr. J. N. Levine Edwards AFB, CA 93523
1	Lockheed Palo Alto Rsch Labs ATTN: Tech Info Ctr 3251 Hanover Street Palo Alto, CA 94304
1	Aerojet Solid Propulsion Co. ATTN: Dr. P. Micheli Sacramento, CA 95813
1	ARO Incorporated ATTN: Mr. N. Dougherty Arnold AFS, TN 37389
1	Atlantic Research Corporation ATTN: Dr. M. K. King 5390 Cherokee Avenue Alexandria, VA 22314
1	AVCO Corporation AVCO Everett Research Lab Div ATTN: D. Stickler 2385 Revere Beach Parkway Everett, MA 02149
2	Calspan Corporation ATTN: Dr. E. B. Fisher A. P. Trippe P.O. Box 235 Buffalo, NY 14221
1	ENKI Corporation ATTN: M. I. Madison 9015 Fulbright Avenue Chatsworth, CA 91311
1	Foster Miller Associates, Inc. ATTN: A. J. Erickson 135 Second Avenue Waltham, MA 02154
1	General Electric Company Armament Department ATTN: M. J. Bulman Lakeside Avenue Burlington, VT 05402
1	General Electric Company Flight Propulsion Division ATTN: Tech Lib Cincinnati, OH 45215
1	Paul Gough Associates, Inc. ATTN: Dr. P. S. Gough P.O. Box 1614 Portsmouth, NH 03801
2	Hercules Incorporated Alleghany Ballistic Lab ATTN: Dr. R. Miller Tech Lib Cumberland, MD 21501
2	Hercules Incorporated Bacchus Works ATTN: Dr. D. Pilcher Dr. R. Simmons Magna, UT 84044
1	IITRI ATTN: Dr. M. J. Klein 10 West 35th Street Chicago, IL 60615
1	Olin Corporation Badger Army Ammunition Plant ATTN: J. Ramnarace Baraboo, WI 53913
2	Olin Corporation New Haven Plant ATTN: R. L. Cook D. W. Riefler 275 Winchester Avenue New Haven, CT 06504

DISTRIBUTION LIST

No. of Copies	Organization
1	Physics International Company 2700 Merced Street Leandro, CA 94577
1	Pulsepower Systems, Inc. ATTN: L. C. Elmore 815 American Street San Carlos, CA 94070
2	Rockwell International Corp Rocketdyne Division ATTN: Dr. C. Obert Dr. J. E. Flanagan 6633 Canoga Avenue Canoga Park, CA 91304
2	Rockwell International Corp Rocketdyne Division ATTN: Mr. W. Haymes Tech Lib McGregor, TX 76657
1	Science Applications, Inc. ATTN: Dr. R. B. Edelman 23146 Cumorah Crest Woodland Hills, CA 91364
1	Shock Hydrodynamics, Inc. ATTN: Dr. W. H. Anderson 4710-16 Vineland Avenue North Hollywood, CA 91602
1	Thiokol Corporation Elkton Division ATTN: E. Sutton Elkton, MD 21921
3	Thiokol Corporation Huntsville Division ATTN: Dr. D. Flanigan Dr. R. Glick Tech Lib Huntsville, AL 35807
2	Thiokol Corporation Wasatch Division ATTN: Dr. John Peterson Tech Lib P. O. Box 524 Brigham City, UT 84302
1	TRW Systems Group ATTN: Dr. H. Korman One Space Park Redondo Beach, CA 90278
2	United Technology Center ATTN: Dr. R. Brown Tech Lib P. O. Box 358 Sunnyvale, CA 94088
1	Universal Propulsion Co ATTN: H. J. McSpadden P. O. Box 546 Riverside, CA 92502
1	Battelle Memorial Institute ATTN: Tech Lib 505 King Avenue Columbus, OH 43201
1	Brigham Young University Dept of Chemical Engineering ATTN: Dr. M. Beckstead Provo, UT 84601
1	California Institute of Tech ATTN: Prof. F. E. C. Culick 204 Karman Lab, Mail Stop 301-46 1201 E. California Street Pasadena, CA 91125
1	Case Western Reserve Univ Division of Aerospace Sciences ATTN: Prof. J. Tien Cleveland, OH 44135

DISTRIBUTION LIST

No. of Copies	Organization
3	Georgia Institute of Technology School of Aerospace Engineering ATTN: Prof. B. T. Zinn Prof. E. Price Prof. W. C. Strahle Atlanta, GA 30332
1	Johns Hopkins University Applied Physics Laboratory Chemical Propulsion Information Agency ATTN: Mr. T. Christian Johns Hopkins Road Laurel, MD 20810
1	Massachusetts Institute of Technology Dept of Mechanical Engineering ATTN: Prof. T. Toong Cambridge, MA 02139
1	Pennsylvania State University Dept of Mechanical Engineering ATTN: Prof. K. Kuo University Park, PA 16801
3	Princeton University Forrestal Campus Library ATTN: Prof. M. Summerfield Dr. L. Caveny Tech Lib P.O. Box 710 Princeton, NJ 08540
2	Purdue University School of Mechanical Engineering ATTN: Prof. J. Osborn Prof. J. D. Hoffman TSPC Chaffee Hall West Lafayette, IN 47906
1	Rutgers State University Dept of Mechanical and Aerospace Engineering ATTN: Prof. S. Temkin University Heights Campus New Brunswick, NJ 08903
1	Southwest Research Institute Fire Research Section ATTN: W. H. McLain P.O. Drawer 28510 San Antonio, TX 78228
1	Stanford Research Institute Propulsion Sciences Division ATTN: Tech Lib 333 Ravenswood Avenue Menlo Park, CA 94024
1	Stevens Institute of Technology Davidson Laboratory ATTN: Prof. R. McAlevy III Hoboken, NJ 07030
1	University of California San Diego AMES Department ATTN: Prof. F. Williams P.O. Box 109 La Jolla, CA 92037
1	University of Illinois Dept. of Aeronautical Engineering ATTN: Prof. H. Krier Transportation Bldg, Rm 105 Urbana, IL 61801
1	University of Minnesota Dept. of Mechanical Engineering ATTN: Prof. E. Fletcher Minneapolis, MN 55455

DISTRIBUTION LIST

No. of Copies	Organization
2	University of Utah Dept. of Chemical Engineering ATTN: Prof. A. Baer Prof. G. Flandro Salt Lake City, UT 84112

Aberdeen Proving Ground

Marine Corps LnO
Dir, AMSAA